ARTICLE Communicated by John Hertz

The High-Conductance State of Cortical Networks

Arvind Kumar
arvind_kumar@brown.edu
Sven Schrader
schrader@biologie.uni-freiburg.de
Ad Aertsen
aertsen@biologie.uni-freiburg.de
Neurobiology and Biophysics, Faculty of Biology, University of Freiburg, D-79104 Freiburg, Germany, and Bernstein Center for Computational Neuroscience, D-79104 Freiburg, Germany

Stefan Rotter
stefan.rotter@biologie.uni-freiburg.de
Theory and Data Analysis, Institute for Frontier Areas of Psychology and Mental Health, D-79098 Freiburg, Germany, and Bernstein Center for Computational Neuroscience, D-79104 Freiburg, Germany

We studied the dynamics of large networks of spiking neurons with conductance-based (nonlinear) synapses and compared them to networks with current-based (linear) synapses. For systems with sparse and inhibition-dominated recurrent connectivity, weak external inputs induced asynchronous irregular firing at low rates. Membrane potentials fluctuated a few millivolts below threshold, and membrane conductances were increased by a factor 2 to 5 with respect to the resting state. This combination of parameters characterizes the ongoing spiking activity typically recorded in the cortex in vivo. Many aspects of the asynchronous irregular state in conductance-based networks could be sufficiently well characterized with a simple numerical mean field approach. In particular, it correctly predicted an intriguing property of conductance-based networks that does not appear to be shared by current-based models: they exhibit states of low-rate asynchronous irregular activity that persist for some period of time even in the absence of external inputs and without cortical pacemakers. Simulations of larger networks (up to 350,000 neurons) demonstrated that the survival time of self-sustained activity increases exponentially with network size.

A.K. and S.S. contributed equally to this work.

1 Introduction

In view of experimental constraints in assessing the activity dynamics of cortical networks in vivo directly, computational models have gained increasing importance in recent years (Vogels, Rajan, & Abbott, 2005). In fact, random recurrent networks of spiking neurons have emerged as a standard theoretical model, subject to both approximate analytical treatment (Amit & Brunel, 1997; Brunel, 2000, 2003) and numerical simulations (Golomb & Hansel, 2000; Mehring, Hehl, Kubo, Diesmann, & Aertsen, 2003). Typically, a recurrent network model of the neocortex comprises two populations of neurons, excitatory and inhibitory ones, equipped with both intra- and inter-population synaptic connections. The dynamics of such networks with current-based (linear) synapses has been investigated in great detail. In the current-based model, postsynaptic potentials arise from stereotyped current transients. Inputs are not affected by the state of the postsynaptic neuron and, in turn, do not change its integrative properties. A more realistic (nonlinear) model of the synapse assumes a stereotyped conductance transient in the postsynaptic membrane instead. Recent experimental (Chance, Abbott, & Reyes, 2002; Destexhe, Rudolph, & Paré, 2003; Shu, Hasenstaub, & McCormick, 2003) and theoretical (Meffin, Burkitt, & Grayden, 2004; Kuhn, Aertsen, & Rotter, 2004) studies of input integration in cortical neurons revealed that synaptic activity can indeed strongly modulate the properties of input integration and, therefore, of neuronal dynamics (Shelley, McLaughlin, Shapley, & Wielaard, 2002; Vogels & Abbott, 2005). First, active synapses on the dendrite decrease the input resistance of the membrane, resulting in a reduced effective membrane time constant. This leads to shorter and attenuated postsynaptic potentials (PSPs). Second, a shift in the mean membrane potential leads to a change of the driving force, which determines the amplitude of postsynaptic potentials. In combination, this yields a nonmonotonic rate transfer function of neurons with conductance-based synapses, in contrast to the monotonic input-output characteristic for neurons with current-based synapses (Kuhn et al., 2004).

While it was clear for a long time that synaptic conductances can influence the integrative properties of single neurons (Bernander, Douglas, Martin, & Koch, 1991; Rapp, Yarom, & Segev, 1992), little is known about their effect on the dynamics of networks. In a recent study, Meffin et al. (2004) showed with analytical methods that a network with conductance-based synapses would indeed reflect important features of single-neuron behavior reported from in vivo intracellular recordings: the membrane time constant is reduced, the mean membrane potential is just below threshold, and small fluctuations induce a low firing rate and irregular firing patterns. The effects of conductance-based synapses on dynamic population activity, however, were not discussed. To address this issue, we systematically studied the dynamics of large, sparse random networks of

integrate-and-fire neurons connected with conductance-based synapses. In particular, following the work of Brunel (2000), we investigated how the activity states of the network depend on the relative strength of inhibition and the intensity of external inputs and what the impact is of synaptic time constants.

A simple mean field model for conductance-based networks suggested the possibility of stable self-sustained activity at low firing rates, even in the absence of external inputs. In large-scale simulations, networks with conductance-based synapses were indeed found to sustain low-rate asynchronous irregular activity, which closely resembles cortical spiking activity in awake, behaving animals. Here we show that by modeling synapses in the network as conductances, a sufficiently large network, once activated to be in a sufficiently stationary state, exhibits self-sustained activity without any internal pacemakers and even after all inputs have been removed. The biological meaning of such self-sustained activity is an open issue, as the intact brain under normal circumstances is constantly receiving input from various sensory and nonsensory channels. However, isolated brain tissue, such as cortical cultures (Plenz & Aertsen, 1996) and deafferented cortical slabs (Burns & Webb, 1979; Timofeev, Grenier, Bazhenov, Sejnowski, & Steriade, 2000), is known to exhibit self-sustained activity in the absence of external input. Such experimental observations could so far be explained only by the action of hypothetical endogenously active neurons (Latham, Richmond, Nelson, & Nirenberg, 2000; Latham, Richmond, Nirenberg, & Nelson, 2000).

Preliminary results of this study have been presented previously in abstract form (Schrader, Kumar, Rotter, & Aertsen, 2005; Kumar, Schrader, Rotter, & Aertsen, 2005).

2 Materials and Methods

2.1 Recurrent Random Networks. We analyzed the dynamics of recurrent random networks of integrate-and-fire neurons. We fixed the size of the networks at $N = 50{,}000$ for most simulations, but networks of up to 350,000 neurons were also considered in this study. We assumed that the larger fraction of all neurons ($N_{\mathrm{exc}} = 0.8\ N$) was excitatory and the rest ($N_{\mathrm{inh}} = 0.2\ N$) inhibitory. Each neuron received input from K neurons from within the network, of which $K_{\mathrm{exc}} = 0.8\ K$ were randomly chosen from the excitatory pool and $K_{\mathrm{inh}} = 0.2\ K$ from the inhibitory pool. Multiple synapses between the same pair of neurons were allowed. The resulting networks were of relatively sparse connectivity, such that K/N was 0.1 or lower. In addition to the recurrent connections, each neuron received K_{ext} external Poisson-type inputs, all excitatory, with a rate ν_{ext} for each afferent. Apart from the type of synapses assigned to them, excitatory and inhibitory neurons were treated identically (see Figure 1). Specific numbers for all simulations shown are collected in Table 1.

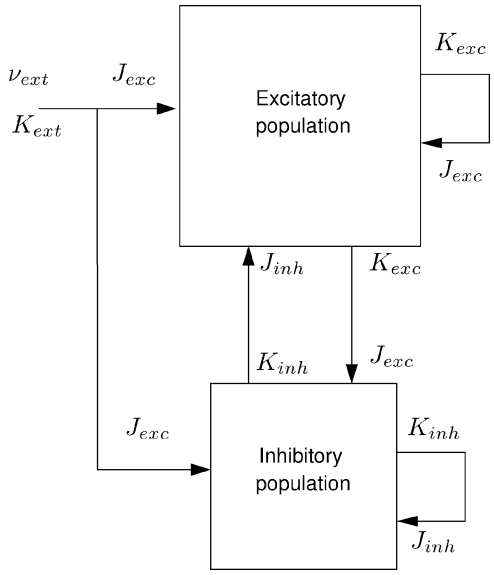

Figure 1: Network architecture. Two populations of N_{exc} excitatory and N_{inh} inhibitory neurons were sparsely connected in a recurrent fashion. Each neuron received input from K_{exc} excitatory and K_{inh} inhibitory neurons within the network. In addition, all neurons had K_{ext} excitatory connections representing nonlocal inputs to the network. The relative strength of inhibitory synapses g and the intensity of external inputs ν_{ext} were the control variables in numerical simulations of network dynamics.

2.2 Integrate-and-Fire Neuron Model. We studied networks of point neurons of the integrate-and-fire (I&F) type. The I&F neuron model is computationally simple (Tuckwell, 1988a; Gerstner & Kistler, 2002) yet captures essential features of input integration and spiking dynamics in real neurons (Rauch, La Camera, Lüscher, Senn, & Fusi, 2003). For this neuron model, the subthreshold dynamics of the membrane potential $V^i(t)$ in neuron i is described by the leaky-integrator equation,

$$C\frac{d}{dt}V^i(t) + G_{\text{rest}}\big[V^i(t) - V_{\text{rest}}\big] = I^i_{\text{syn}} \tag{2.1}$$

where I^i_{syn} is the total synaptic input current into neuron i. The resting potential was set to $V_{\text{rest}} = -70$ mV. The parameters $C = 250$ pF and $G_{\text{rest}} = 16.7$ nS lead to a membrane time constant of $\tau_{\text{rest}} = C/G_{\text{rest}} = 15$ ms, reflecting the electrical properties of the neuronal membrane in the absence of any synaptic input. We implemented a deterministic threshold-reset mechanism for spike generation (Tuckwell, 1988a, 1988b), assuming a fixed

spike threshold of 20 mV above rest ($V_\theta = -50$ mV). After the membrane potential reached threshold, a spike was emitted, the membrane potential was reset to its resting value, and synaptic integration was halted for 2 ms, mimicking the refractory period in real neurons. To be able to record the "free" membrane potential (Kuhn et al., 2004) in selected neurons of the network, we "cloned" them (letting them receive the same input as their respective twins) and switched off spiking in the clone. Apart from this deviation for technical reasons, all model neurons had identical parameters.

2.3 Conductance-Based Synapses. In this study, synaptic input was modeled by transient conductance changes, using alpha functions (Jack, Noble, & Tsien, 1975; Rotter & Diesmann, 1999):

$$G(t) = \begin{cases} J\,\frac{t}{\tau}e^{1-\frac{t}{\tau}} & \text{for } t \geq 0 \\ 0 & \text{for } t < 0. \end{cases} \tag{2.2}$$

We refer to the peak amplitude J of the conductance transient, which is assumed at $t = \tau$ after onset, as the "strength" of the synapse. Generally, excitatory and inhibitory synapses had different strengths J_{exc} and J_{inh} assigned. Both excitatory and inhibitory synapses, however, had in general identical time constants of $\tau_{\text{exc}} = \tau_{\text{inh}} = 0.326$ ms. This value was obtained by fitting excitatory postsynaptic potentials (EPSPs) with alpha-shaped excitatory postsynaptic currents (EPSCs) to the parameters of empirical EPSPs, assuming a membrane time constant of 10 ms. This yielded rise times (time to peak) of about 1.7 ms and a half-width at half-height of about 8.5 ms for EPSPs at rest. These values were close to what was reported from acute slices of cat visual cortex (Fetz, Toyama, & Smith, 1991). To explore the impact of this parameter for network dynamics, most simulations were repeated for $\tau_{\text{exc}} = \tau_{\text{inh}} = 0.978$ ms (three-fold slower) and 1.63 ms (five-fold slower). For certain questions, we also employed combinations of different time constants for excitation and inhibition in our simulations.

The total excitatory conductance $G^i_{\text{exc}}(t)$ in neuron i was given by

$$G^i_{\text{exc}}(t) = \sum_{j=1}^{K_{\text{exc}}+K_{\text{ext}}} \sum_k G_{\text{exc}}\big(t - t^j_k - D\big). \tag{2.3}$$

The outer sum runs over all excitatory synapses onto this particular neuron, and the inner sum runs over the sequence of spikes arriving at a particular synapse. Similarly, the total inhibitory conductance $G^i_{\text{inh}}(t)$ in neuron i was given by

$$G^i_{\text{inh}}(t) = \sum_{j=1}^{K_{\text{inh}}} \sum_k G_{\text{inh}}\big(t - t^j_k - D\big). \tag{2.4}$$

A uniform transmission delay of $D = 1.5$ ms was imposed for all synapses and in all simulations. The total synaptic current into neuron i was

$$I^i_{\text{syn}}(t) = -G^i_{\text{exc}}(t)\big[V^i(t) - V_{\text{exc}}\big] - G^i_{\text{inh}}(t)\big[V^i(t) - V_{\text{inh}}\big], \tag{2.5}$$

where $V_{\text{exc}} = 0$ mV and $V_{\text{inh}} = -80$ mV are the reversal potentials of the excitatory and the inhibitory synaptic currents, respectively. The ratio

$$g = \frac{J_{\text{inh}}\tau_{\text{inh}}|V_{\text{rest}} - V_{\text{inh}}|}{J_{\text{exc}}\tau_{\text{exc}}|V_{\text{rest}} - V_{\text{exc}}|} \tag{2.6}$$

was used to parameterize the relative strength of effective inhibition. For fast conductance transients and small amplitudes, it corresponds approximately to the ratio of inhibitory postsynaptic potential (IPSP) and EPSP peak amplitudes at rest. It is important to point out, however, that the inhibition-excitation ratio g (originally introduced for current-based models) has a slightly different meaning for the conductance-based synapse model. Being a quotient of peak potentials in previous work (Brunel, 2000), here g is approximately the ratio of total charges induced at rest.

It should also be noted that in the case of conductance-based synapses, the effective time constant of the neuron depends on the input and can strongly deviate from the membrane time constant $\tau_0 = C/G_{\text{rest}}$ without input (Kuhn et al., 2004). Active synapses contribute to the total membrane conductance, thereby also changing the membrane time constant. In this way, the integrative properties of the neuron depend on its input, and the model becomes nonlinear. This effect is not present in models where synapses are modeled as current sources.

2.4 Parameters Used in Network Simulations. Here we give a list of the various parameter sets used in different simulation series. See section 3 for more detailed explanations.

Table 1: Parameters Used in the Network Simulations.

		Used for Figures		
Parameter	Unit	2–7, 9	10–12	13
N	1	50,000	10,000–200,000	70,000–350,000
K	1	5000	2000	2000
K_{ext}	1	4000	0	0
J_{exc}	nS	0.68	6	2–10
J_{inh}	nS	4.8–48	95	20–200

2.5 Numerical Simulations. In previous work on current-based networks, two parameters were found to critically influence the dynamic state of the network: the intensity of external inputs ν_{ext} and the relative strength of recurrent inhibition g (Brunel, 2000). We performed numerical simulations of conductance-based networks for different values for ν_{ext} and g and characterized the resulting network dynamics. We also examined the influence of the network size N on various parameters describing its activity.

The computational demands for numerical simulation of large recurrent networks (beyond 10,000 neurons, say) are exceedingly high with respect to both computing power and memory, and it may be impossible to conclude the simulations in reasonable time on a single-processor machine. We performed the simulations on parallel computers (IBM Regatta SMP and AMD Opteron cluster) using a parallelized kernel of NEST (Diesmann & Gewaltig, 2002; Morrison, Mehring, Geisel, Aertsen, & Diesmann, 2005). The simulation technology used in our study allowed us to simulate networks of up to 350,000 neurons with 700 million synapses, which is about the size of a cortical "column".

The dynamic equations were integrated using the GSL implementation of the adaptive fourth-order Runge-Kutta method (Abramowitz & Stegun, 1964; Press, Teukolsky, Vetterling, & Flannery, 1992; Galassi et al., 2001). The temporal resolution of integration was 0.1 ms with an imposed precision of 0.001 mV. All networks were simulated for at least 2 s, but if firing rates fell below 10 spikes per second, we extended our simulations to up to 20 s to collect enough spikes for statistical analysis. In all simulations, an initial period of 300 ms was discarded to avoid possible onset transients of the network activity.

External inputs were generally implemented as independent Poisson processes; each neuron received input from a private source, and all sources were assumed to be independent. Technically, in parallel simulations, it was important to employ appropriate algorithms to obtain long, uncorrelated sequences of pseudo-random numbers for different seeds (Knuth, 1997; Morrison, Mehring, et al., 2005).

2.6 Characterizing Network Dynamics. To characterize the dynamical states of simulated network activity at the level of both single neurons and populations, we employed the following descriptors.

Irregularity of individual spike trains was measured by the squared coefficient of variation of the corresponding interspike interval (ISI) distribution:

$$\text{CV}_{\text{ISI}}^2 = \text{Var}[\text{ISI}]/\text{E}[\text{ISI}]^2. \tag{2.7}$$

Low values reflect more regular spiking; a clocklike pattern yields $\text{CV}_{\text{ISI}}^2 = 0$. $\text{CV}_{\text{ISI}}^2 = 1$ indicates Poisson-type behavior. As a measure for irregularity in the network, we used the average irregularity across all neurons.

Synchrony for a pair of neurons is typically measured by the correlation coefficient of the joint spike counts C_i and C_j:

$$\mathrm{Corr}[C_i, C_j] = \mathrm{Cov}[C_i, C_j]/\sqrt{\mathrm{Var}[C_i]\mathrm{Var}[C_j]}. \tag{2.8}$$

Here, time bins of width 2 ms were used. Note that correlation coefficients may strongly depend on the bin size chosen for analysis (Tetzlaff et al., 2007). Absolute values of correlation must therefore be carefully interpreted with this caveat in mind. A systematic variation of bin size for various network states showed that for certain network states, there is a plateau that guarantees some degree of robustness of the measured values. Also, bins in the range 1 to 5 ms are commonly used in the experimental literature. As a measure for synchrony of population activity in the network, we employed the average correlation coefficient for 250 disjoint pairs of neurons (CC_S).

3 Results

Neuronal spike trains in the neocortex of awake, behaving animals are generally characterized by a high degree of irregularity in their ISIs and a large variability of spike counts (Softky & Koch, 1993; Nawrot, Riehle, Aertsen, & Rotter, 2000). The firing rates of single neurons are generally low (Abeles, Vaadia, & Bergman, 1990; Brecht & Sakmann, 2002), and the correlations in the spiking of pairs of neurons are small (Abeles, 1991; Vaadia & Aertsen, 1992), rendering the ongoing (spontaneous) activity asynchronous. Embedded in an active network of this type, cortical neurons are continuously exposed to recurrent synaptic input. The joint action of excitatory and inhibitory inputs keeps the membrane potential mostly below threshold, and small fluctuations cause the neuron to spike irregularly (Gerstein & Mandelbrot, 1964; Shadlen & Newsome, 1998). A self-consistent description of this scenario for recurrent networks has been subject of several modeling studies (van Vreeswijk & Sompolinsky, 1998; Brunel, 2000). It was found that random recurrent networks of I&F neurons exhibit distinct activity states, depending on the intensity of external excitatory inputs and the relative strength of recurrent inhibition. The firing pattern of individual neurons can be either regular (R) or irregular (I), population activity is either synchronous (S) or asynchronous (A), and the network assumes one of four possible characteristic states (AI, SI, AR, or SR; Brunel, 2000). Of these, it is the AI regime where network activity is considered to most closely resemble cortical spiking activity in vivo (Softky & Koch, 1993). Both experimental evidence (Destexhe et al., 2003; Leger, Stern, Aertsen, & Heck, 2005) and theoretical arguments (Bernander et al., 1991; Rapp et al., 1992; Kuhn et al., 2004) indicate that massive synaptic bombardment strongly alters the integrative properties of individual neurons in a particular way, mainly caused

by a reduction of the membrane resistance associated with synaptic activity ("high conductance state"; Destexhe et al., 2003). Currently, however, there is only partial understanding of how the phenomena on the level of neurons and networks are linked to each other.

3.1 Dynamic States of Network Activity. Conductance-based networks, like current-based networks, show a variety of different behaviors as a function of the control parameters ν_{ext} and g, ranging from highly synchronized firing of the entire neural population to nearly asynchronous population activity, with single neurons firing at either high or low rates, producing either regular or irregular firing patterns. Figure 2 depicts four characteristic examples, covering all possible combinations of properties except the AR state, which was never encountered.

3.1.1 Irregularity and Synchrony of Network Activity. We used "irregularity" to characterize single-neuron spike trains and "synchrony" to capture correlations within the population. Figure 3 depicts cross-covariances and interval densities for the same network states as shown in Figure 2. The squared coefficient of variation (CV_{ISI}^2) is a straightforward way to measure the width of the interval density in a way that corrects for the firing rates. We used the average squared coefficient of variation as a measure for irregularity in the network. The shape of the oscillatory cross-covariance functions motivated our choice of 2 ms for the width of the bins, from which we computed the count correlation coefficient for individual pairs of neurons. The average count correlation coefficient over a sample of 250 pairs (CC_{S}) was used as a measure for synchrony in the network.

When these two measures are used, network activity can be essentially classified into four different states, as done for current-based networks (Brunel, 2000). Based on our numerical simulations, we systematically evaluated these statistical descriptors, in addition to firing rate and membrane potential statistics, as a function of the control parameters g and ν_{ext}. The results are shown in Figure 4. Note that in our parameter scans, different values of g were realized by fixing some value for J_{exc} and varying J_{inh} accordingly (see Table 1). This is not meant to imply that the behavior of the network did not depend on the specific choice of J_{exc} or τ_{exc}, and an independent variation of the strength of excitation and inhibition was performed later (see Figure 13).

For low values of inhibition ($g < 1.5$), neurons spiked at high rates and exhibited synchronous activity. Both the firing rate and synchrony increased as the external input was increased (see Figures 4a and 4c). A single frequency dominated the population signal even for asynchronous activity. For large parts of the parameter space, the dominant frequency was between 100 Hz and 200 Hz (data not shown), enclosing the frequency $\frac{1}{4D} = 167$ Hz that is generally expected for a system with a uniform intrinsic

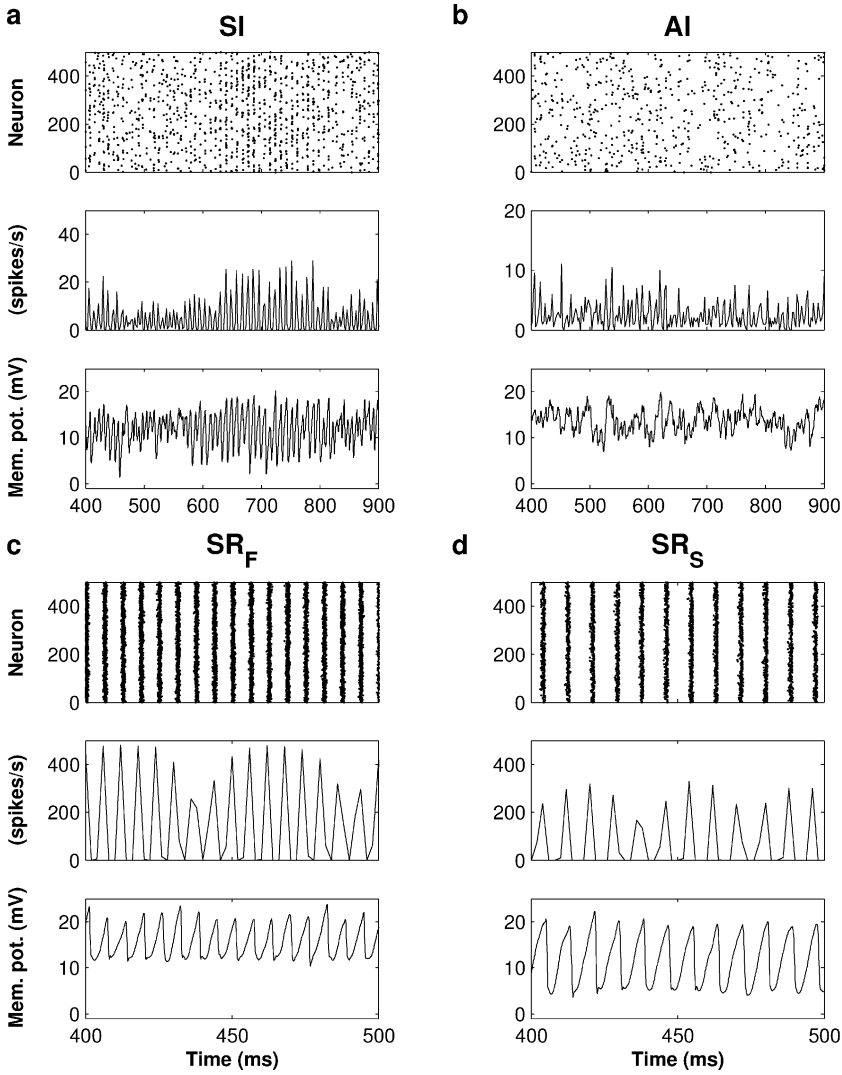

Figure 2: Different types of cortical network activity. Shown are samples of (a) synchronous irregular (SI), (b) asynchronous irregular (AI), (c) synchronous regular fast (SR_F), and (d) slow (SR_S) activity. In each subplot, the upper panel shows the spike trains of 500 excitatory neurons recorded from a network of $N = 50{,}000$ neurons (see Table 1 and Figure 4 for parameters). The middle panel depicts the peristimulus time histogram (PSTH) of the population, normalized for the number of neurons and the histogram bin with (1 ms), yielding the average single-neuron firing rate. Note the very different rates in the four different states. The lower panel displays the free membrane potential of a randomly selected single neuron.

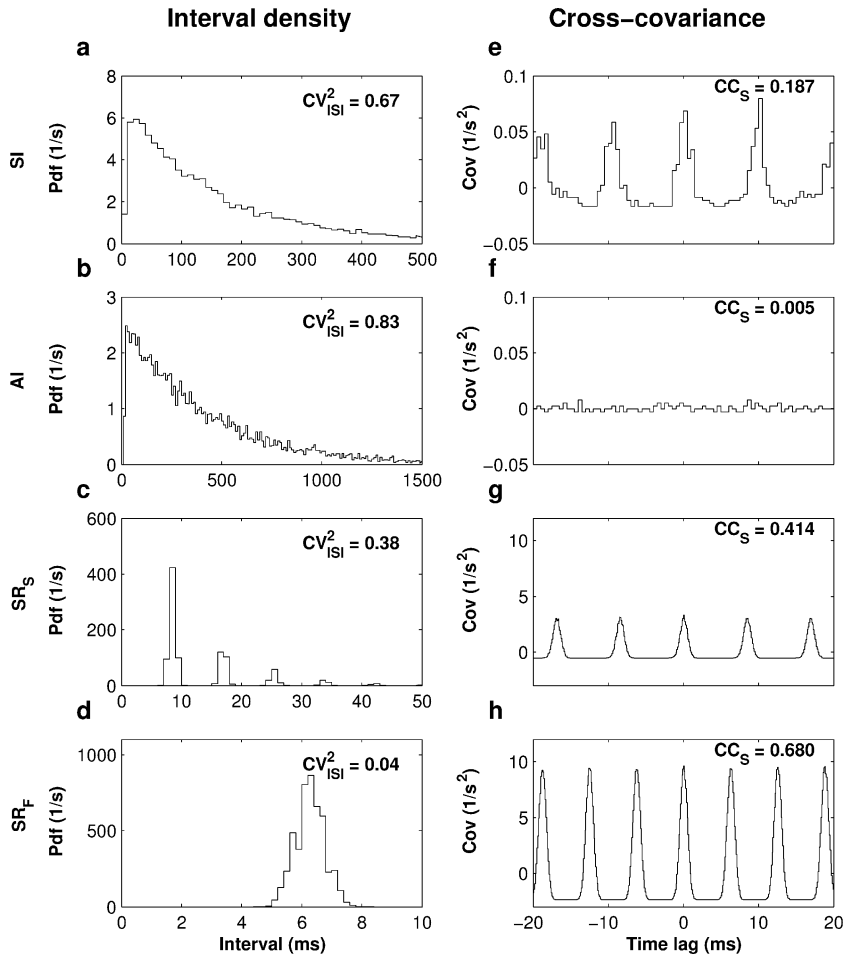

Figure 3: Irregularity and synchrony. These two descriptors of network activity are related to the interspike interval densities (left) and the spike count cross-covariances (right), respectively. Shown are samples of (a, e) synchronous irregular (SI), (b, f) asynchronous irregular (AI), (c, g) synchronous regular slow (SR_S), and (d, h) synchronous regular fast (SR_F). Samples, as in Figure 2. To describe the dynamic state of the network, irregularity was defined as the squared coefficient of variation (CV^2_{ISI}) of the interspike intervals, averaged over all neurons in the network. Synchrony was defined as the count correlation coefficient for counting windows of width 2 ms, averaged over a random sample of 250 neuron pairs (CC_S). For details, see section 2.

delay $D = 1.5$ ms (Murray, 2002; Brunel, 2000; Brunel & Wang, 2003; Maex & De Schutter, 2003; Roxin, Brunel, & Hansel, 2005). Single-neuron firing patterns were regular (see Figure 4d). The mean free membrane potential was closely below threshold, which was 20 mV above rest (see Figure 4e).

As the relative strength of inhibition was increased ($g > 1.5$), the mean membrane potential always remained subthreshold, and firing was driven by fluctuations in the membrane potential. This resulted in quite irregular firing at low rates (less than 10 spikes/s). For not too high values of ν_{ext}, the network generally exhibited asynchronous population activity. In contrast, high synchrony at higher firing rates (more than 50 spikes/s) was observed for all values of g in the explored range if the external input ν_{ext} exceeded 5 spikes per second.

The neurons in all network states observed in our simulations had strongly increased membrane conductances due to massive synaptic

---

Figure 4: Characteristics of network activity. The dynamical states of a large recurrent network (here, $N = 50{,}000$) can be classified by jointly considering several observables, as shown here for different configurations defined by the control parameters g and ν_{ext}. The labels SI, AI, SR_{F}, and SR_{S} indicate the combinations of parameters underlying the samples shown in Figure 2 (see Table 1 for parameters). (a) All of the neurons in the network fire essentially at the same rate. Shown is the mean across a population of 500 randomly selected neurons. The contour lines correspond to a mean rate of 5 and 60 spikes per second, respectively. (b) The total conductance of the neuronal membrane is strongly increased relative to the leak conductance ($G_{\text{rest}} = 16.7$ nS) for all network states examined here. For AI states, conductances are increased by a factor 2 to 5, leading to a corresponding reduction of the membrane time constant from $\tau_{\text{rest}} = 15$ ms to a value of 3 to 8 ms, in accordance with physiological findings. Shown are mean values for a sample of three neurons recorded during a network simulation of 1.7 seconds duration. The white contour circumscribes the asynchronous regime (see *c*), the black contour the irregular regime (see *d*). (c) The level of synchrony in the network (measured by the mean pairwise correlation; see section 2) was strongly dependent on ν_{ext}, and to some degree also on g. The black contour indicates a value of 0.01 and the white contour a value of 0.1 for the synchrony. (d) The irregularity of the spike trains (measured by the mean normalized variance of the interspike intervals; see section 2), by contrast, was more or less uniform in the inhibition-dominated regime ($g > 1.5$). In the excitation-dominated regime ($g < 1.5$), however, neurons produced quite regular spike patterns. The contours indicate a value of 0.8 for the irregularity. (e, f) The mean (above rest) and the standard deviation of the free membrane potential, respectively, for a randomly chosen neuron. The contours in both panels are the same, indicating a mean free membrane potential of 12 mV and 15 mV above rest, respectively. The spike threshold was at 20 mV above rest.

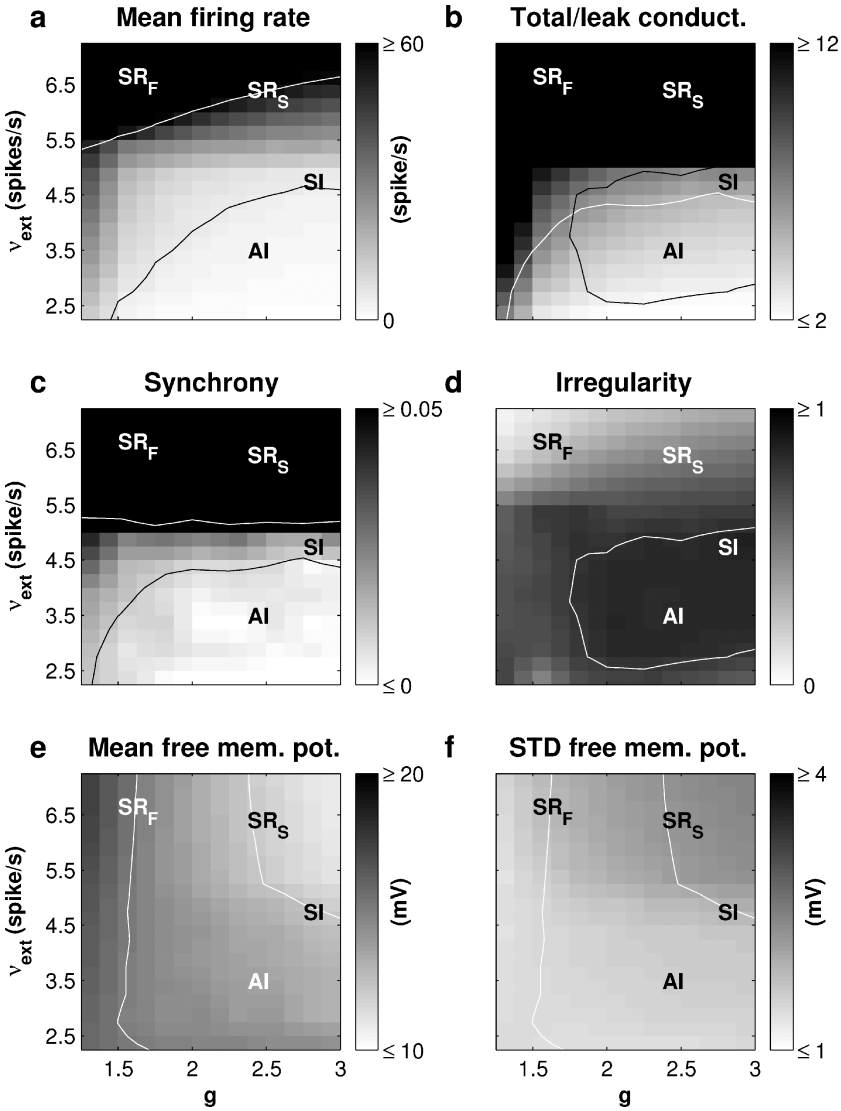

bombardment (see Figure 4b). For states that exhibit high network synchrony, the observed values were higher than what is normally found in healthy cortical neurons. AI-type states, in contrast, were accompanied by an increase of the total membrane conductance by a factor of 2 to 5 and a corresponding reduction of the membrane time constant from $\tau_{\text{rest}} = 15$ ms to a value of 3 to 8 ms. These results are in very good agreement with physiological observations in vivo (Destexhe et al., 2003; Leger et al., 2005).

Our results on single-neuron spiking and population activity in networks with conductance-based synapses are roughly in line with previous observations in current-based networks (Amit & Brunel, 1997; Brunel, 2000; Mehring et al., 2003).

However, we found important differences in the membrane potential statistics of individual neurons during the AI state of the network. In the current-based model, the mean membrane potential is often close to the resting potential, while spikes are induced by quite large fluctuations in the membrane potential due to recurrent input. By contrast, in our simulations of networks with conductance-based synapses, we found that in the AI state, the mean membrane potential of neurons is only about 5 mV below spike threshold, and the firing is driven by relatively small fluctuations (see Figures 4e and 4f). In fact, the membrane potential of neurons recorded intracellularly in vivo is also close to threshold, and spiking is induced by small fluctuations (Destexhe et al., 2003; Leger et al., 2005). This indicates that the membrane potential dynamics in the current-based network model tends to reflect a nonphysiological state of the individual model neurons. By contrast, for the conductance-based model, both the network dynamics and the membrane potential dynamics are in very good accordance with extracellular and intracellular measurements in vivo.

In networks with current-based synapses, the transition from high-activity states to low-activity states occurs for a fixed amount of recurrent inhibition at $g_{\mathrm{crit}} = K_{\mathrm{exc}}/K_{\mathrm{inh}}$, independent of external input and network activity. For conductance-based networks, by contrast, the transition happens for relatively low values of g, provided the inputs are weak (see Figure 4a). For higher values of ν_{ext}, high firing rates (100 spikes/s or more) occur in conjuction with high synchrony in the network, and this combination is barely affected by the strength of recurrent inhibition (see Figures 4a and 4c).

3.1.2 Postsynaptic Potentials in Active Networks. One of the prominent effects of modeling synapses as conductance transients is the significant reduction of membrane impedance and effective membrane time constant for strong inputs, which attenuates and shortens the postsynaptic potentials (Kuhn et al., 2004). To further characterize synaptic integration, it is interesting to account for effective PSP amplitudes in an active network. Experimentalists typically use spike-triggered averaging (STA) to estimate the effective size and shape of PSPs (Fetz et al., 1991; Matsumura, Chen, Sawaguchi, Kubota, & Fetz, 1996; Dayan & Abbott, 2001). We also performed such STA in our simulations; the results are shown in Figures 5a and 5b. The drawback of this method is that if inputs are correlated, the trigger spike may systematically co-occur with spikes from other neurons also impinging on the target neuron. This may result in a strong bias for the PSP estimate, skewing the PSP amplitude distribution toward larger values and leading to complex, often multimodal waveforms. In addition, the

STA method requires a large number of trigger spikes to obtain a reliable estimate.

In our simulations, we modified the STA protocol to circumvent these problems. Two almost identical simulations of the network were performed. The second run was different from the first one only insofar as the cloned, nonspiking neurons (see section 2) received some extra excitatory and inhibitory inputs, each firing at an arbitrarily chosen frequency of 2 spikes per second and uncorrelated with both the external and the recurrent inputs to this neuron. Obviously these extra inputs had no effect on the network dynamics, since these neurons contributed no spikes to the network. By subtracting the membrane potential trace recorded in the first simulation from the trace recorded in the second simulation, we could cleanly isolate 150 EPSPs and 150 IPSPs that arose during network activity. The PSPs obtained in this way did reflect input-dependent membrane impedance and depolarization-dependent driving force, without being contaminated by input correlations (see Figures 5c and 5d for some samples). For obvious reasons, this method of estimating PSP amplitudes unfortunately cannot be employed in physiological experiments.

In one particular scenario, the strength of synapses was chosen such that the EPSP amplitude distribution in the active network roughly matched the distribution reported from intracellular recordings in vivo (Matsumura et al., 1996; Hasenstaub et al., 2005). This was achieved for EPSPs at $J_{\mathrm{exc}} = 0.68$ nS, which lead to an amplitude of 0.15 mV for the resulting unitary EPSP at rest, when no other inputs were active. However, it yielded heterogeneous but systematically lower amplitudes in active neurons due to the shunting effect of many active synapses and a reversal potential for excitation at 0 mV. The strength of inhibition was adjusted to bring the network close to an AI state with firing rates around 7 spikes per second. This was achieved for $J_{\mathrm{inh}} = 12$ nS, corresponding to $g = 2.5$. (For $g = 1$, the amplitude of unitary IPSPs at rest, that is, in the absence of other inputs, was equal to the amplitude of EPSPs.) Consequently, and also due to the reversal potential for inhibition around rest, IPSPs attained much higher amplitudes than EPSPs for depolarized membrane potentials. Figures 5e and 5f show histograms of PSP amplitudes measured in one particular simulation. The median amplitude of unitary EPSPs recorded in the AI state was 0.12 mV, close to the mean EPSP amplitude measured in awake, behaving monkeys (Matsumura et al., 1996). The distribution of EPSP amplitudes (see Figure 5e) that resulted from our simulations, however, did not exhibit a long tail as seen in the in vivo experiments, possibly because the potential effect of input correlations in the estimation procedure was excluded by our protocol. Note that for relatively fast PSCs, the case considered here, the PSP amplitude is only weakly affected in the high-conductance state. Slower PSPs would experience a (much) stronger reduction in amplitude (Kuhn et al., 2004). Estimated IPSP amplitudes were about five times larger than those of the EPSPs. Also, the distribution of IPSP amplitudes (see

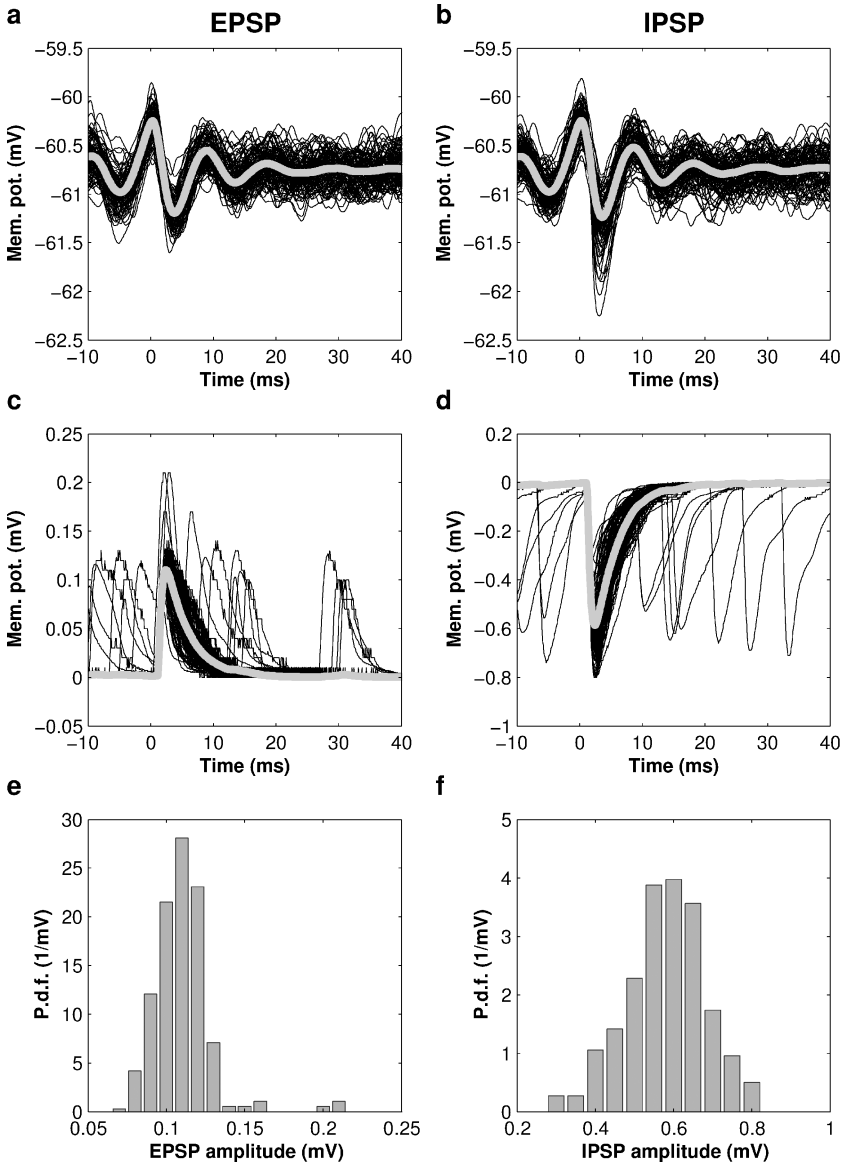

Figure 5f) was much wider than that of the EPSPs. Note that in our simulations of the AI state, IPSPs were generally much stronger than reported in the experiments (Matsumura et al., 1996). Trading in the strength of the inhibitory synapses for increased firing rates of inhibitory neurons, as suggested by physiological studies (McCormick, Connors, Lighthall, & Prince,

1985; Connors & Gutnick, 1990; Markram et al., 2004), could possibly bring the model again in line with the in vivo data (see also section 4).

3.1.3 Stability of Network Dynamics. A stable system will produce bounded output for bounded input (BIBO). In a series of numerical simulations, we probed the stability of various network states by applying perturbations of the respective external input. We found that the network generally responded quickly to a perturbation regardless of its strength, in both the population activity and the firing of individual neurons. Although strong perturbations could drive the system into synchronous states accompanied by network oscillations, the system always rapidly relaxed back to its equilibrium as the perturbation was removed. Figure 6 shows raster plots and population activity histograms for two representative simulations. In both cases, the network was initially in the AI state, and its reaction to step-like perturbations of different strengths (see Figure 6e) was explored. The effect of a relatively weak perturbation (increasing the intensity of external Poissonian inputs from 3.5 spikes/s to 4.5 spikes/s per neuron; Figures 6a and 6b) was hardly visible in the population response, and the network remained in the asynchronous irregular state with only slightly increased firing rates. For a stronger perturbation (external input of 5.5 spikes/s per neuron; Figures 6c and 6d), the network was driven into a synchronous state with rather high firing rates. Nevertheless, after removing the extra input, the network relaxed back to its original state in both cases, without any indication of hysteresis or other memory effects. We conclude from such experiments that the network is generally stable in the BIBO sense, even for quite strong perturbations.

Figure 5: Effective EPSP and IPSP amplitudes in the AI state. Parameters were extracted from a network simulation, where external inputs fired at 2 spikes per second, the neurons in the network had a mean firing rate of about 7 spikes per second, and the mean free membrane potential of neurons was approximately 5 mV below threshold (see Table 1 for parameters). (a, b) One hundred traces of membrane potential cutouts (black) of one neuron in the network, triggered by the spikes of other neurons that were randomly picked from the network. Averages (gray) were based on on 1000 such trigger events. These standard spike-triggered averages were strongly affected by correlated spiking in the network, and even neuron pairs that were not synaptically coupled exhibited nonzero averages. To circumvent this problem, a variant of the method was employed here, yielding isolated PSPs (c, d; see text for details). Depicted are again individual cutouts (black) and averages (gray) over 700 EPSPs and 400 IPSPs, respectively. Such modified spike-triggered averages were used to generate normalized histograms of effective EPSP and IPSP amplitudes. Bin width was 8.3 μV and 40 μV, respectively.

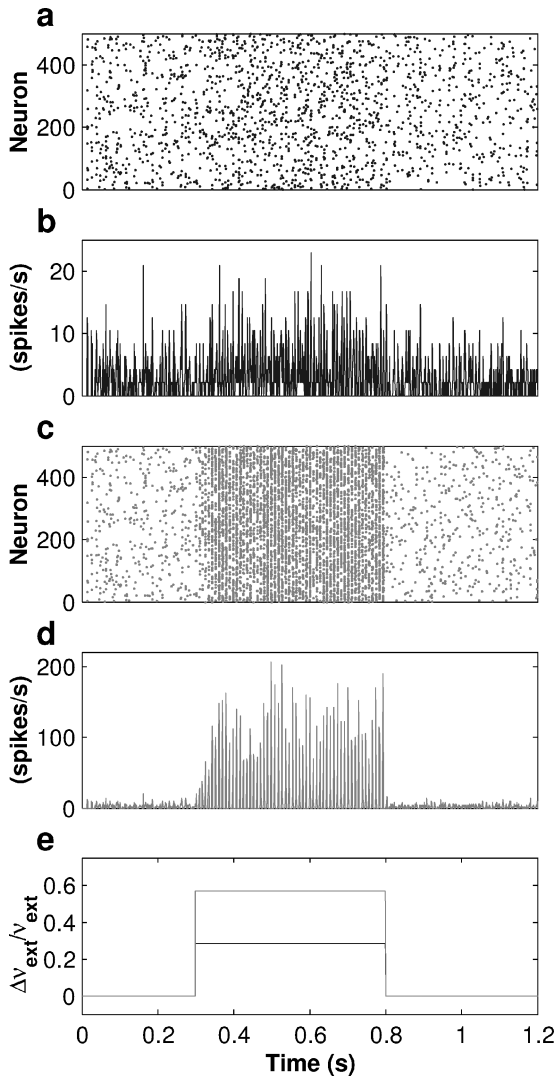

Figure 6: Stability of network states. To probe the stability of a network state ($g = 2.5, \nu_{\text{ext}} = 3.5$), equilibrium activity was perturbed by some extra excitatory input $\Delta\nu_{\text{ext}}$, using the temporal protocol shown in *e*. Shown are typical responses from a network (see Table 1 for parameters) on weak (black) and strong (gray) perturbations, where the latter drove the network into synchronous states. Depicted are raster displays of 500 excitatory neurons (a, c) and the corresponding population PSTHs (b, d; bin width 1 ms) of the whole network. In both cases, network activity rapidly increased as the extra input was switched on; as the extra input was switched off, network activity rapidly returned to its original level again. This behavior indicates BIBO stability (see text for more details).

3.1.4 Effect of Synaptic Time Constants. Up to now, we have considered networks where excitatory and inhibitory synaptic conductances had equally small time constants ($\tau_{exc} = \tau_{inh} = 0.326$ ms). This choice was in approximate accordance with measurements in acute cortical slices (Fetz et al., 1991). The only available in vivo study, however, reported PSP rise times and PSP widths for both excitation and inhibition that were more than three-fold larger than in vitro (Matsumura et al., 1996). Other in vitro studies accounted for inhibitory synaptic time constants that were larger than the excitatory ones (Tarczy-Hornoch, Martin, Jack, & Stratford, 1998; Williams & Stuart, 2003). In this section we explore the effect of either larger time constants for both EPSCs and IPSCs, and of unequal time constants for EPSCs and IPSCs, on the activity states of the network. To study the effect of an altered time constant in isolation, we compensated the increase in τ_{exc} and/or τ_{inh} by a reduced amplitude of G_{exc} and/or G_{inh}, respectively. This kept the effective strength of the synapse (total area of the synaptic conductance transient; see section 2.3) constant. Figure 7 shows the state space of the network as a function of g and ν_{ext} in analogy to Figure 4, for several different scenarios involving equal time constants for excitation and inhibition (see Figures 7b and 7c), and for inhibition that is slower than excitation (see Figures 7d and 7e).

Generally the simultaneous increase of the time constants of both excitation and inhibition by a factor 3 (see Figure 7b) or 5 (see Figure 7c) did not induce great changes in the state space as far as it was scanned, except for a slightly increased gain of the network for external inputs. By contrast, an increase of the time constant of inhibition alone while keeping excitation fast (see Figures 7d and 7e) resulted in an increase of the firing rates as compared to the symmetric case (see Figures 7a to 7c). This indicates that by increasing τ_{inh}, the impact of the inhibitory population within the recurrent network is reduced. In fact, in earlier work, we could already show that in general, slow PSPs are more strongly attenuated in the high-conductance state than fast PSPs (Kuhn et al., 2004). Typically, for large, balanced random networks, high firing rates are associated with both more regular interspike intervals of single neurons and more synchronous population activity (see Figure 4). The same was observed when inhibition was made slower: both regularity and synchrony in the network increase with the increased firing rates (see Figures 7d and 7e). When τ_{inh} was increased by a factor of 5 as compared to τ_{ext} (see Figure 7e), population activity was synchronized for the whole range of g and ν_{ext} studied here. This raises the question whether low-synchrony states can be achieved in networks with slow inhibition provided the rates are low. We approached this question in a scenario where low rates were achieved by increasing the relative amount of recurrent inhibition, leaving the synaptic time constants untouched. For values of $g = 10$, the IPSP amplitudes were approximately 1.5 mV at rest, which is in the range of amplitudes typically observed in in vitro (Tarczy-Hornoch et al., 1998; Williams & Stuart, 2003). However, as Figures 7d and 7e suggest, the AI state of the network cannot be "restored" by a simple inhibitory

compensation. Within the range of parameters studied here numerically, we found that the network does not support AI-type activity if inhibition is too slow.

3.2 Mean Field Approach to Network Dynamics. Analytical solutions for models of recurrent networks of spiking neurons are difficult to obtain and involve several approximations (Brunel, 2000). Numerical simulations of large networks, on the other hand, are both time and memory consuming. For current-based networks, the global dynamics of random networks could be successfully characterized in terms of single-neuron dynamics using mean field theory (Amit & Brunel, 1997). Here we employed a similar approach for conductance-based networks and compare the results to simulations of large networks. Studying networks by resorting to a single-neuron approximation has several distinct advantages: It avoids some of the approximations that have to be made for analytical treatment, while at the same time significantly reducing the computational load.

For the scenario studied here, individual neurons operate in the fluctuation-driven regime, that is, the mean membrane potential remains subthreshold, and spikes are mostly elicited by transients of the membrane

---

Figure 7: Effect of slower synaptic time constants on network behavior. The same type of network was studied here as shown in Figure 4, except for increased, but still equal, time constants of excitatory and inhibitory synapses (b, three-fold; c, five-fold) or, alternatively, for increased time constants of inhibitory synapses alone (d, three-fold; e, five-fold). In all cases the effective strength of individual synapses (total induced charge) was unchanged. Three characteristic parameters of network activity were studied: mean firing rate (left), synchrony of the network (middle), and irregularity of single-neuron firing (right) as a function of g and ν_{ext}. Note the greatly extended range for the parameter g in all panels, as compared to Figure 4. Generally the simultaneous increase of the time constants for both excitation and inhibition by a factor of up to 5 did not induce great qualitative changes in the network behavior as far as the parameter space was scanned, except for a slightly increased gain of the network for external inputs (b, c). In contrast, slowing inhibition selectively generally increases the firing rates in the network (d, e, left). The two contour lines in the left panels correspond to firing rates of 60 spikes per second (white) and 5 spikes per second (black), respectively. In parallel to the increase in rate, the degree of synchrony in the network is also increased (middle). The contour line represents an average pairwise correlation coefficient of 0.01. For very slow inhibition, however, such low values of synchrony are practically absent in the parameter space considered here. Similarly, slower inhibition induces more regular single-neuron spike trains (right). The white contour line indicates a value of 0.7 for the squared coefficient of variation.

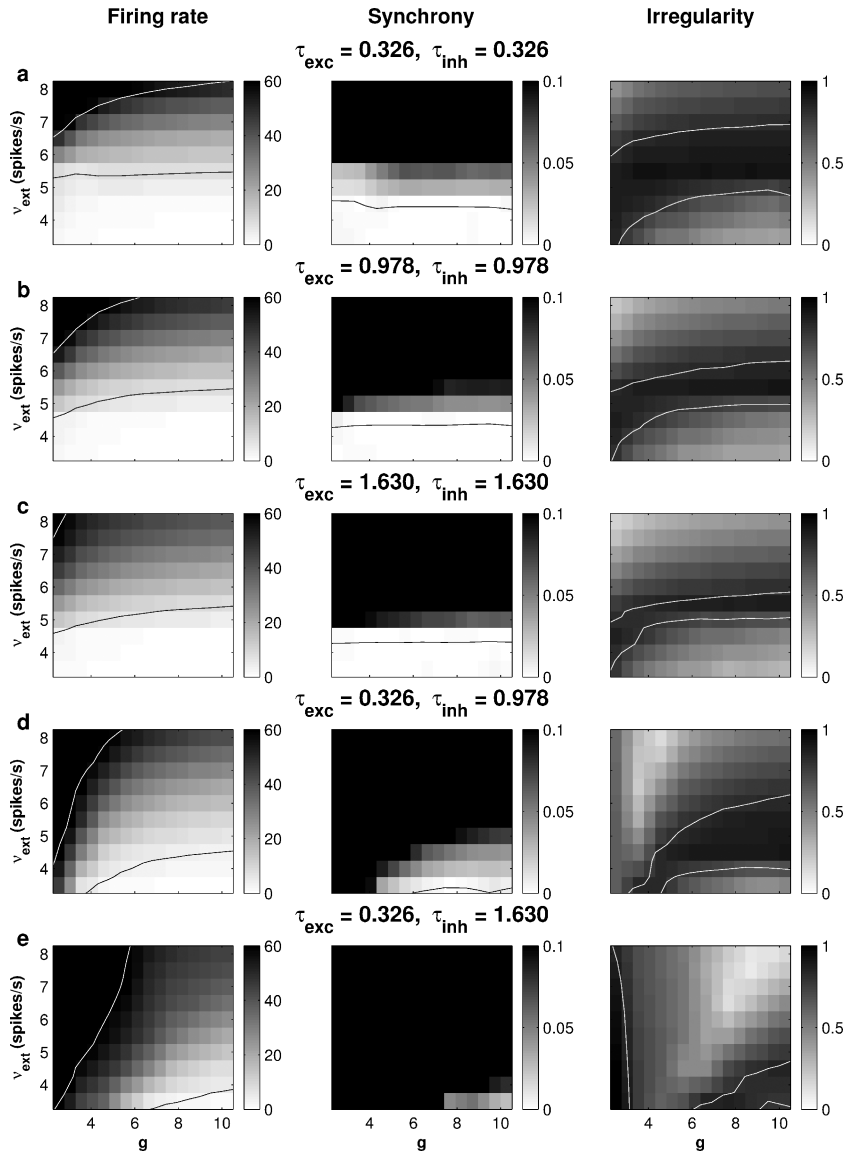

potential toward threshold. The amplitude of these transients (i.e., the standard deviation of the membrane potential distribution) increases with the rate of inputs, and it depends on both the amplitude and the width of individual postsynaptic potentials. In fact, both amplitude and width of the PSPs are reduced for smaller input impedances and shorter effective

membrane time constants. It is well within the physiological range of input rates that the reduction of the output rate due to synaptic shunting wins over its increase by increasing input rates. As a result, neurons with conductance-based synapses may exhibit nonmonotonic input-output curves (Kuhn et al., 2004). This feature has interesting consequences for the behavior of recurrent networks.

3.2.1 Self-Consistent Firing Rates. A neuron being part of a network receives three types of inputs: K_{ext} connections from nonlocal excitatory neurons, each spiking at rate ν_{ext}; K_{exc} connections from local excitatory neurons, each spiking at rate ν_{exc}; and K_{inh} connections from local inhibitory neurons, each spiking at rate ν_{inh} (see Figure 8a).

There are two dynamical variables in this model, ν_{exc} and ν_{inh}, whereas ν_{ext} and g play the role of control parameters. In a homogeneous network, however, all neurons receive approximately the same input and, as a consequence, produce output spikes at about the same rate. It is therefore reasonable to assume that local excitatory and inhibitory neurons are spiking at the same rate $\nu_{exc} = \nu_{inh} = \nu_{net}$. In the mean field scenario, all inputs to a neuron are modeled as independent Poisson-type spike trains (respecting synaptic multiplicities), which is adequate for networks in the AI state. The output of the neuron has rate ν_{out}. For each pair of values for ν_{ext} and g, the input-output rate transfer function f describing ν_{out} as a function of ν_{net} characterizes the response properties of the neuron.

Assuming self-consistency in the corresponding recurrent network, ν_{out} should in fact be equal to ν_{net} for any given pair of values for ν_{ext} and g. We estimated both the rate transfer function and the rate fixed point based on numerical simulations (see Figure 8b). Note that some constellations of parameters may yield not only two fixed points—one for nonzero

---

Figure 8: Mean field approach to network dynamics. (a) Single-neuron scenario to study the behavior of a network where all neurons have the same connectivity parameters. All neurons in the network receive K_{exc} local excitatory and K_{inh} local inhibitory inputs, which are assumed to fire all at the same rate ν_{net}. The relative strength of inhibitory couplings is given by the parameter g. Each neuron receives in addition K_{ext} external excitatory inputs, each spiking at rate ν_{ext}. (b) Single-neuron transfer functions, determined by numerical simulations. Shown is the firing rate of a neuron (black curves) that received input from $K_{exc} = 1{,}600$ excitatory and $K_{inh} = 400$ inhibitory Poisson neurons firing each at rate ν_{net}; external inputs were silent (see text). Depicted are the transfer functions for two different scenarios. Assuming stationarity, self-consistent activity in a recurrent network implies that input rates and output rates are equal (dashed diagonal). The corresponding fixed points of the transfer function (here at about 15.4 spikes/s and 34.5 spikes/s, respectively) could be determined with high precision from numerical simulations.

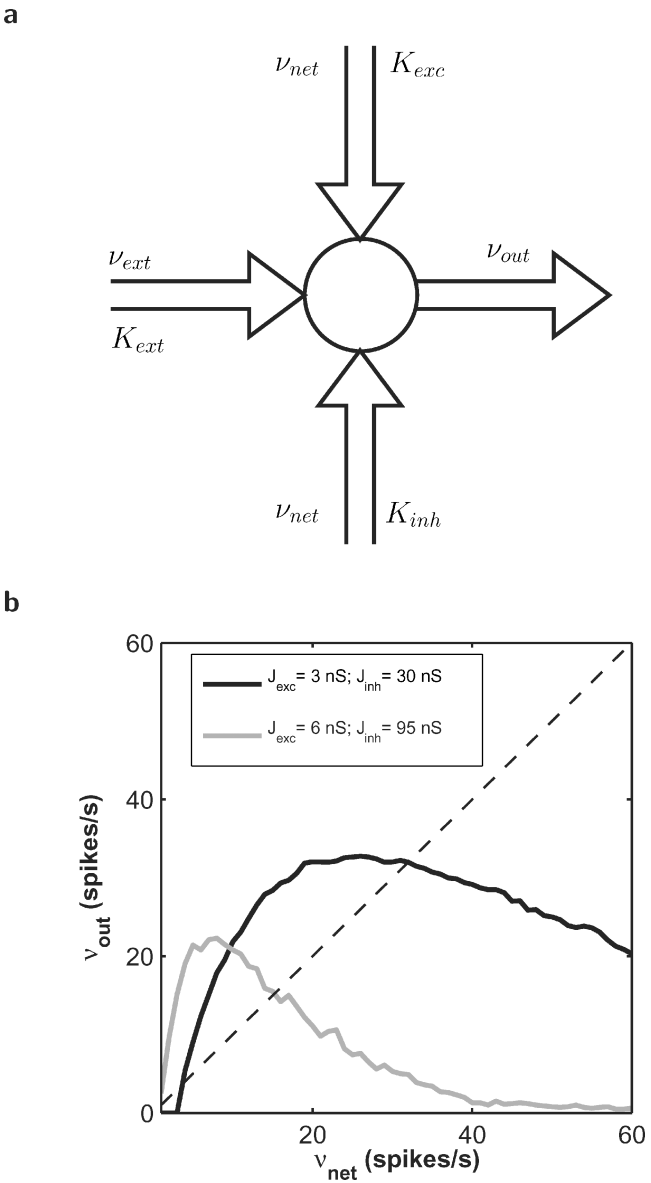

firing rates and the "trivial" one for zero rate (gray curve)—but a third one for some in-between rate (black curve). The two fixed points common to most input-output curves are typically attracting, whereas the potential third fixed point is normally repelling. It indicates a threshold for recurrent

activity below which the network quickly falls into silence. Simulations also yielded good estimates for the irregularity of spiking and for the mean and the standard deviation of the free membrane potential (not shown).

3.2.2 Comparison with Recurrent Network Dynamics. Figure 9 shows that the mean field model provided an excellent approximation of the AI-type activity with respect to neuronal firing rates for large parts of the (g, ν_{ext}) parameter regime studied here. Deviations (see Figure 9c) arose due to several effects, the two most important of which are discussed below (see also Brunel, 2000).

Shared connectivity in the network may lead to correlations in the recurrent input (Kuhn, Aertsen, & Rotter, 2003), which were not captured by the independent Poisson inputs assumed in the mean field model. In a sense, the mean field model assumes a network of infinite size, where shared connectivity and, hence, input correlations are not present. Likewise, inputs with a regularity that deviates from that of a Poisson process may also affect the output. Thus, our numerical mean field approach could be improved by accounting for the effect of non-Poissonian irregularity or of input correlations in the network activity underlying the neuronal transfer functions.

3.3 Self-Sustained Activity in Recurrent Networks. From anatomical studies, it is known that the number of sensory input fibers is very small compared to the number of neurons in the cortex, not to speak of the number of cortico-cortical connections (Braitenberg & Schüz, 1998). In fact, real-time optical imaging and single-unit recordings in the cat visual cortex in vivo showed considerable, spatially organized activity even in the absence of a visual stimulus (Arieli, Sterkin, Grinvald, & Aertsen, 1996). The neurons involved in such ongoing activity fire action potentials at relatively low rates (below 5 spikes/s) (Abeles, 1991; Latham et al., 2000; Chiu & Weliky, 2001). This activity component has been termed "ongoing" activity, expressing that it presumably reflects dynamic brain processes beyond the direct effect of a sensory stimulus. Also, isolated brain tissue, such as cortical cultures (Plenz & Aertsen, 1996) or deafferented cortical slabs (Burns & Webb, 1979; Timofeev et al., 2000), were found to be able to retain some spiking activity. Although it is well possible that spontaneously active neurons (e.g., pacemaker cells in the thalamus) initiate activity in the otherwise silent cortex (Latham et al., 2000), it is nevertheless an interesting question whether cortical networks can also maintain stable spiking at low rates by means of their massive recurrent connections (Amit & Brunel, 1997; Salinas, 2003; Shu et al., 2003). For theoretical reasons, derived from the analysis of simple firing rate models, it has been claimed that stable self-sustained activity within the AI regime is impossible (Latham et al., 2000). Recently, however, the question was raised whether conductance based networks can behave differently (Kuhn et al., 2004; Schrader et al., 2005; Kumar et al., 2005; Vogels

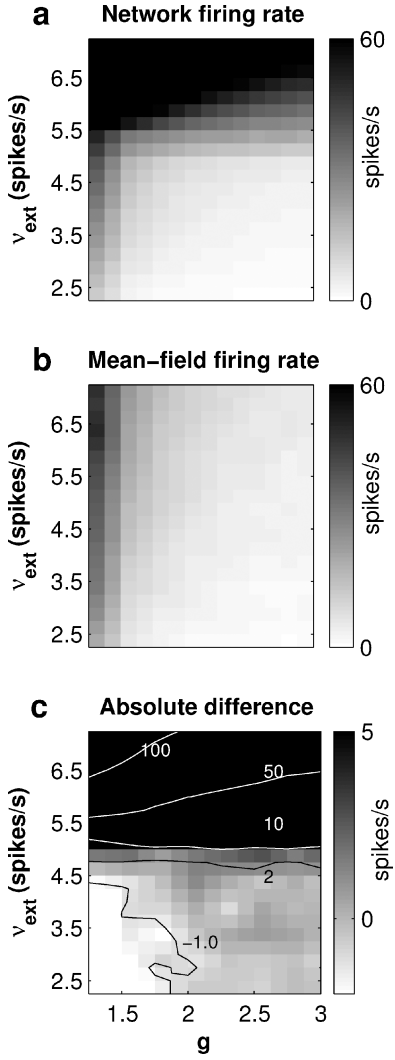

Figure 9: Mean field theory versus network simulations. (a) Average firing rates estimated from network simulations for different combinations of external input ν_{ext} and relative strength of inhibition g. (b) Firing rates at the fixed point in single-neuron simulations, where network inputs were replaced by independent Poisson inputs (mean field). (c) Absolute difference between the average firing rate measured in network simulations (a) and the firing rate obtained from mean field theory (b). As long as the network is in the asynchronous irregular regime (see Figure 4), the single-neuron approximation predicts the firing rates in the network very well. However, networks in the excitation-dominated regime ($g < 1.5$) or networks with strong external inputs ($\nu_{ext} > 4.5$) exhibit synchronous activity, and the mean field prediction fails to match the network simulations.

& Abbott, 2005). In particular, Kuhn et al. (2004) observed that neurons with synaptic conductances exhibited a nonmonotonic response characteristic when driven by balanced input. They speculated that for suitable network architectures, this nonmonotonic dependence would predict the existence of stable self-sustained network activity in the absence of external inputs. Here we show that by modeling synapses in the network as conductances, a sufficiently large network, once activated to be in a sufficiently stationary state, shows self-sustained activity without any internal pacemakers, even after all inputs have been removed.

3.3.1 Establishing Self-Sustained Activity. The particular form of the input-output characteristic of conductance-based neurons leads to the prediction of stable self-sustained network activity. The gray curve in Figure 8b depicts the transfer function of such a neuron, illustrating the existence of a nontrivial fixed point. Next to a fixed point at zero rate (assuming zero input or pacemaker neurons), a second point exists where input and output rates are consistent, at relatively low rates. While some fixed points are unstable since small perturbations drive the activity away from it, others are attractive, and after small perturbations, the activity relaxes back to its equilibrium (see Figure 6). Thus, as long as the mean field scenario provides a meaningful approximation to the recurrent network dynamics, we would indeed expect self-sustained spiking at low rates, even without pacemaker neurons, and in the absence of any external drive.

Network simulations largely confirmed this prediction from mean field theory. The obvious approach to reach this activity state in a network simulation would be to provide external input until all neurons are firing at a rate close to the desired self-consistent rate. The intrinsic stability of this state would then let the network settle at its fixed point, even after switching off the external inputs. Note that the mean firing rate in the network does not decrease, since the reduction in synaptic bombardment received by each individual neuron is fully compensated by an increase in the amplitude of membrane potential fluctuations due to an increased impedance. It turned out, however, that an abrupt change of the input conditions leads to strong transients in the network activity, compromising its stability. To avoid this effect, we used slowly decaying inputs after having reached stationary firing at the fixed-point rate (see Figure 10c). Under these circumstances, the network remained active for some period of time, even after the external input was completely removed (see Figures 10a and 10b). The population mean of self-sustained activity in the example shown was 13.9 spikes per second, which was slightly below the fixed-point at 15.4 spikes per second derived from mean field theory. Possible reasons for this deviation are discussed below. In principle, self-sustained activity can also be established at higher firing rates. For the analysis presented here, however, we concentrated on networks that exhibit AI-type activity at low rates.

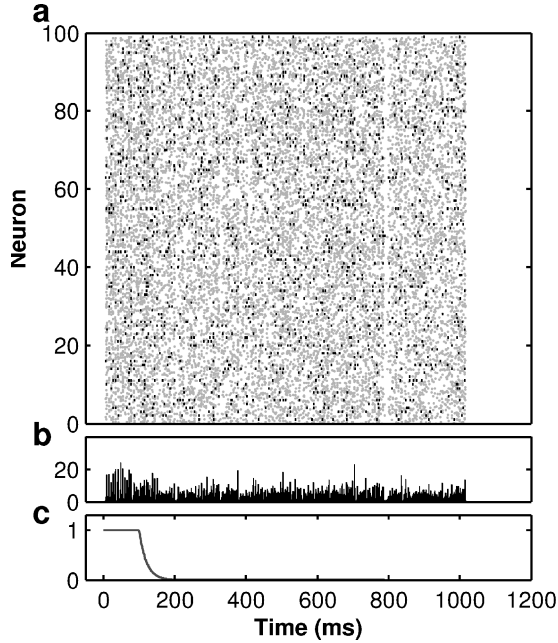

Figure 10: Self-sustained activity in conductance-based networks. Inducing self-sustained activity in a network comprising $N = 30{,}000$ neurons (see Table 1 for parameters). External input was necessary only to ignite network activity; here we used external inputs firing at a rate of 1 spike per second per neuron. When stationary firing had established itself (here after 100 ms), external input was gradually decreased (exponential decay, time constant 50 ms). Interestingly, the network remained active. In the example shown, self-sustained activity ceased spontaneously after about a second. The small spontaneous "population burst" that terminated self-sustained activity presumably induced too much inhibition for the network to remain active. (a) Spiking activity of 100 (black ticks) and 1000 (gray dots) excitatory neurons randomly selected from the network. (b) Peristimulus time histogram depicting the firing rate (spikes/s) averaged over all neurons in the network (bin size 1 ms). (c) Temporal protocol for the firing rates (in spikes/s) of the external inputs.

3.3.2 Survival of Self-Sustained Activity. In simulations we observed that the networks could sustain their active state for a certain period of time. Typically this self-sustained activity ended by a "spontaneous" transition to the zero-rate state (see Figure 10). What determines the survival time of (nonzero) persistent network activity?

The main assumption underlying the mean field approach taken here is the independence of input channels for each neuron. In a recurrent network, however, the finite size of the system and the unavoidable overlap of input

populations for different neurons introduce correlations of network activity. It is known that such correlations may affect the individual neurons' firing rates (Kuhn et al., 2003). Independent of this single-neuron effect, the fluctuations of population activity in the network may also be strongly increased due to pairwise or higher-order correlations. For example, the vertical "stripes" in the raster display of Figure 10a, which indicate near-synchronous firing of many neurons, are the result of complex recurrent interactions among the 30,000 neurons constituting this particular network. If (transient) synchronization indeed caused the spontaneous death of our networks, larger networks should then be less vulnerable, since correlations due to overlapping inputs are bound to be weaker.

We investigated this issue in more detail by performing a series of simulations in which we systematically varied the network size. Since it is the number of inputs to each neuron that determines its firing rate under self-consistent conditions, this parameter was held constant while increasing the number of neurons in the network. Under these constraints, large networks necessarily have a sparser connectivity than small networks. A statistical assessment of the influence of network size on the survival of self-sustained activity is shown in Figure 11.

The mean firing rate of individual neurons did not change with network size (see below), in all cases falling slightly short of the value predicted by mean field theory. This invariance was consistent with the fact that the size of the network is irrelevant for the mean field prediction. As expected, however, larger networks indeed exhibited a smaller degree of global synchronization (data not shown). Accordingly, the estimated survival probability clearly increased with network size (see Figure 11a), as expressed by a marked increase of the mean survival time (see Figure 11b). As is typical for rare events, the statistics roughly followed that of a Poisson process, implying exponential lifetime distributions.

The gain of stability for networks with reduced correlation suggested that spontaneous synchronized events may eventually kick the network into a state outside the basin of attraction of the fixed point. More specifically, we hypothesized that moments of excessive synchrony may be followed by a supercritical period of global silence from which the network might not be able to recover. This hypothesis was indeed supported by our simulations (see Figure 10b), where self-sustained activity was found to typically end after a particularly strong, transient population event. In turn, most synchronous events beyond a certain amplitude (peaks in Figure 10b) were followed by a short period of complete silence. This was presumably due to the combined effect of hyperpolarized membrane potentials in many neurons after a spike of their own, followed by a large number of inhibitory events coactivated with the population burst. Our observations were once more emphasized by a comparison of 90 cases of "spontaneous death" with the same number of transient epochs of very low activity ("near-death": fewer than 0.05 spikes per second for 1 ms). The event-triggered time histograms

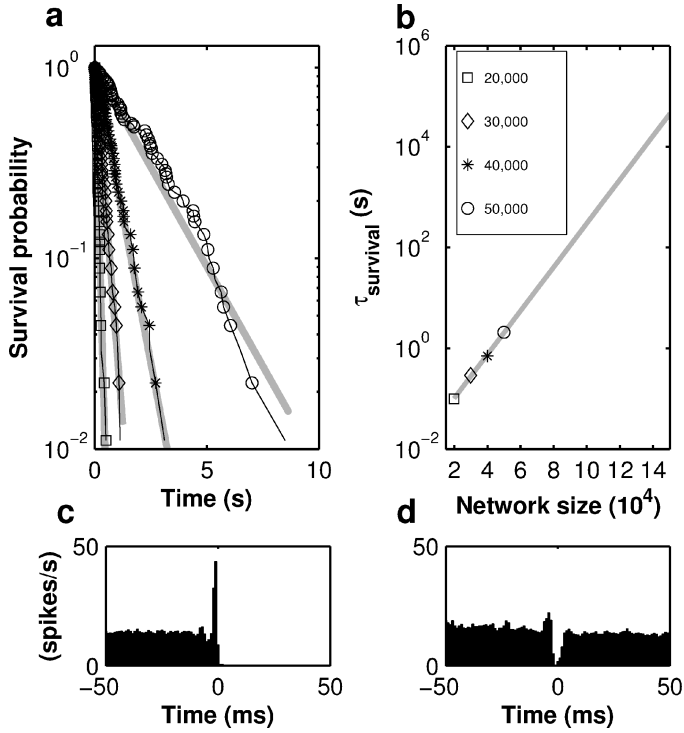

Figure 11: Survival probability of persistent activity increases for larger networks. (a) Survival probability estimated from multiple simulations of large conductance-based networks. For each network size (N = 20,000/30,000/40,000/50,000 neurons) numerical simulations (black symbols) were performed, all based on the same connectivity parameters (see text and Table 1). Resorting to the mean survival time τ_{survival} from 90 simulations for each network size, the data fit an exponential distribution $\mathrm{P}(\tau > t) = \exp(-t/\tau_{\text{survival}})$ very well (gray line). (b) Mean survival time τ_{survival} for different network sizes. The exponential increase in survival probability for larger networks suggests a stabilizing influence of large populations with less shared input. Extrapolation predicts a lifetime on the order of 1 hour for networks as large as a single cortical column. Population PSTHs (bin size 1 ms) were generated from 90 simulations of a network with $N = 30{,}000$ neurons, triggered either (c) on its spontaneous death or (d) on subcritical short periods of relative silence ("near death" with mean rate < 0.05 spikes/s for at least 1 ms). The much higher peak(s) in *c* supports an explanation of spontaneous death in terms of "lethal synchrony" (see text for more details).

(see Figures 11c and 11d) revealed that on average, spontaneous death was preceded by a much stronger transient of population activity than an epoch of near-death from which the network could still recover. We conclude that self-sustained activity in networks with high connectivity is less stable than in sparse networks due to the relative abundance of synchronous population events.

Another parameter affecting the stability of self-sustained AI-type activity is the firing rate assumed at the fixed point. We found that networks operating at higher persistent rates are less susceptible to spontaneous death, presumably because input fluctuations tend to average out and thus are less likely to drive the network out of the stable regime. Similarly, stability at low rates could be achieved only in large networks with many inputs to each neuron. We also found that self-sustained activity at a given rate is less stable for stronger synapses. In this case, the detrimental effects of spontaneous synchronizations were stronger and therefore more often had the power to silence the entire network.

The following simple consideration explains both the increased stability at higher firing rates and the (roughly) exponential growth of survival times with network size. For asynchronous states, all neurons fire independently at rate ν. The probability p for each neuron to fire within a critical window of size T_{crit} is then approximately given by $p = \nu\, T_{\text{crit}}$. The number of neurons k firing within T_{crit} has a binomial distribution $B(p, N, k)$ with mean Np and variance $Np(1-p)$. Assume that the network enters a lethal zone if the active population is increased by a critical factor $\alpha_{\text{crit}} > 1$ with respect to its mean size. The probability that at least $N_{\text{crit}} = \alpha_{\text{crit}} Np$ neurons in the network fire a spike within the critical window is $p_{\text{death}} = \sum_{k=N_{\text{crit}}}^{N} B(p, N, k)$. This probability decreases with increasing rates ν, and it decreases (almost) exponentially for increasing network size N. (This can be easily seen if the binomial distribution is approximated by a normal distribution with the same mean and variance.) Therefore, the corresponding survival times $T_{\text{crit}}/p_{\text{death}}$ increase accordingly. A least-squares fit of the measured mean survival times yielded $p \approx 0.0217$, $\alpha_{\text{crit}} \approx 1.097$, and $T_{\text{crit}} = p/\nu \approx 1$ ms.

3.3.3 Residual Synchrony in the AI State? The role played by residual synchrony during AI-type self-sustained activity in recurrent networks was found to deserve special attention. Two different aspects were considered here. The first concerned the possible influence of synchronization induced by common input. The second examined the possibility of artificial synchronization due to the finite temporal resolution of our simulations.

Networks of $N = 50{,}000$ neurons can be considered large in the sense that they do not change their behavior qualitatively when further increased while leaving the absolute numbers of inputs constant. Smaller networks ($N \leq 30{,}000$) exhibit slightly lower rates, presumably due to the effect of residual synchrony (see above). Very small networks ($N \leq 10{,}000$) with

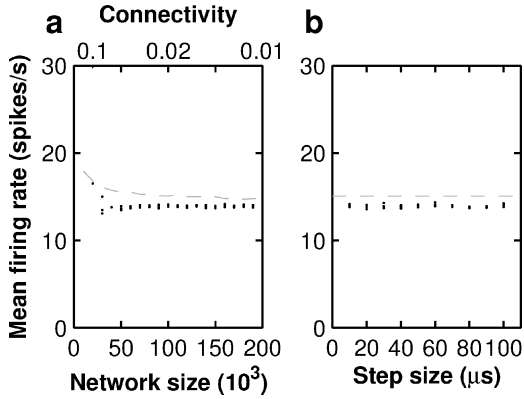

Figure 12: Testing the role of synchrony in AI-type self-sustained activity. In all simulations (black dots) we considered networks with the same number of recurrent inputs per neuron ($K_{\text{exc}} = 1,600$, $K_{\text{inh}} = 400$) and with synapses of the same strength ($J_{\text{exc}} = 6$ nS, $J_{\text{inh}} = 95$ nS). The mean firing rate was found to be independent of (a) the network size N and connectivity K/N (fixed simulation step size 0.1 ms) and of (b) the time step used in the simulations (fixed network size $N = 100{,}000$). In both cases, the mean firing rate was, however, systematically falling slightly short of the firing rate predicted by the fixed point of the mean field approach (dashed line). This is probably caused by synchrony induced by the global oscillations due to transmission delays rather than by direct synaptic coupling or common input (see text).

physiologically plausible synaptic strengths typically are not able to self-sustain activity at all. In networks with more than $N = 50{,}000$ neurons, however, the AI state of recurrent dynamics is largely compatible with the assumption of independently firing neurons. This can be concluded, among other things, from the agreement of our network simulations with the predictions from mean field theory.

A small residual discrepancy between the two, however, was observed in all our simulations of self-sustained activity in the AI state. The most important reasons for this have been discussed above. For large networks, however, we were able to rule out that the deviation was due to correlations induced by common input, not accounted for by mean field theory. To this end, we simulated networks of increasing size N, leaving the total number of recurrent inputs (see Table 1) to each neuron untouched. This resulted in a series of networks of decreasing connectivity K/N and decreasing correlations among neurons due to overlapping input populations. For each of these networks, however, the same mean field model applied. Figure 12a depicts the clear result of this numerical experiment: Network size and connectivity did not affect the measured self-sustained rate, for networks larger than about $N = 50{,}000$ neurons.

All network simulations have to be performed in discrete time steps, the size of which has to be adapted to the time constants of the system under consideration. This is an important step to guarantee simulation results with controlled precision (Rotter & Diesmann, 1999). Temporal resolution, however, is associated with yet another problem in network simulations. Due to the fact that spikes are "forced" to the time grid used for simulation, a certain degree of artificial synchronization is introduced to the system (Hansel, Mato, Meunier, & Neltner, 1998; Morrison, Hake, Straube, Plesser, & Diesmann, 2005). Since even weak synchrony can exert strong effects on the network dynamics, it is important to make sure that the integration step size was chosen small enough to avoid such artefact. Figure 12b demonstrates that for the networks considered here, integration time steps of 0.1 ms were indeed adequate.

3.3.3 Independent Variation of Excitation and Inhibition. Instead of fixing the strength of excitatory synapses J_{exc} and varying the relative strength of inhibition g as was done before, we also considered different combinations of J_{exc} and J_{inh} giving rise to the same value of the inhibition-excitation ratio g. This was done in particular to find out which aspects of self-sustained network activity depend on only the quotient of the synaptic amplitudes, and to which degree the parameter g is 'generic' for conductance-based networks. Figure 13 illustrates various aspects of spiking in a random recurrent network without external inputs, for a wide range of combinations of J_{exc} and J_{inh}, but imposing the same time constants for excitatory and inhibitory synapses ($\tau_{\mathrm{exc}} = \tau_{\mathrm{inh}} = 0.326$ ms). As expected, the average rate during self-sustained firing (see Figure 13a) generally increased with increasing excitation and decreased with increasing inhibition. Contours of constant firing rate were, to some approximation, straight lines through the origin, confirming that the mean rate in the network essentially depends on the ratio g, not on the absolute values of the synaptic strengths.

The discrepancy between self-sustained network rates and the rates predicted by the mean field model is shown in Figure 13b. Generally the rate deviations were fairly small for the range of synaptic strengths considered here. In the more synchronous regime (see Figure 13d), the network fired quite fast; in fact, it fired up to 6 spikes per second faster than predicted. In principle, such accordance between fast and synchronous firing is in agreement with single-neuron studies (Kuhn et al., 2003; Bohte, Spekreijse, & Roelfsema, 2000; Stroeve & Gielen, 2001). However, as implied by Figure 12a, the synchrony is induced by the global oscillations due to common input and transmission delays rather than by direct synaptic coupling. The irregularity of single-neuron firing (see Figure 13c) was found to systematically decrease with increasing firing rates. In turn, low firing rates lead to highly irregular (Poisson-like) spike trains, as observed in other network models of spiking neurons during slow, asynchronous activity (Brunel, 2000; Mehring et al., 2003).

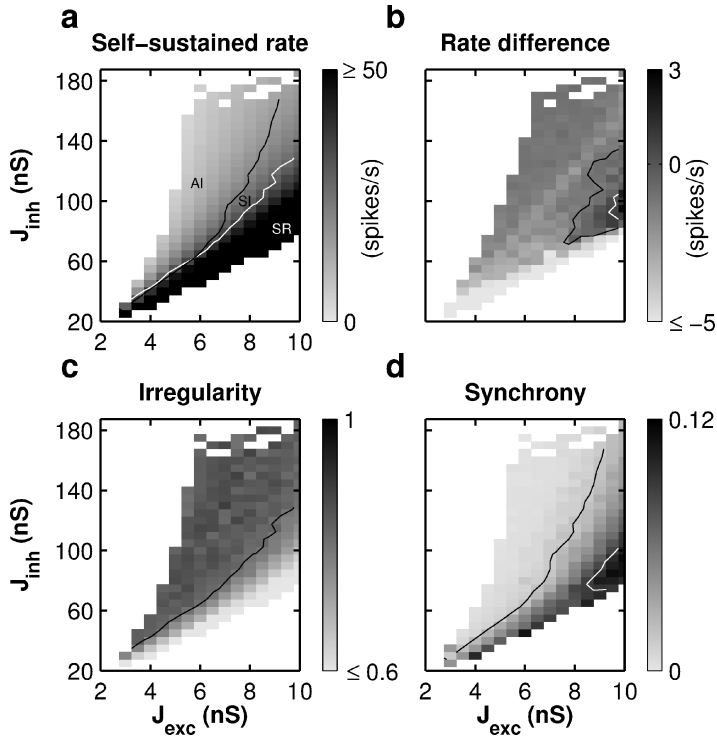

Figure 13: Independent variation of synaptic excitation and inhibition. The analysis was based on 1 s periods of self-sustained activity in large networks with $N = 70{,}000$ neurons. For very strong synapses, however, sufficient stability was achieved only for larger networks with up to $N = 350{,}000$. (a) Average firing rate of neurons during self-sustained network activity. Only networks with firing rates in the range 3.9 to 180 spikes per second were considered. The contours separate the synchronous from the asynchronous (black contour) and the regular from the irregular (white contour) regime; see below. (b) Discrepancy of firing rates in the network with respect to the predictions by mean field theory. Dark areas indicate faster and bright areas slower firing than predicted (white contour, +1 spikes/s; black contour, −1 spikes/s). (c) Irregularity of spike trains (CV^2_{ISI}) averaged across 1000 neurons. The black contour indicates a value of 0.8 for irregularity, as in Figure 4. In regions of very low rates (e.g., for strong synapses), this parameter could not be reliably determined. (d) Mean pairwise correlation (CC_S) for 10,000 randomly selected pairs of neurons recorded during self-sustained activity. The black contour indicates a value of 0.02 for synchrony, as in Figure 4. Note that the region of relatively high synchrony (white contour at 0.095) coincides with the region where the firing rates deviated most from the mean field model assuming independent Poisson inputs.

In this study, only fixed-point rates below 180 spikes per second were considered, avoiding the regime of regular activity. We generally found that self-sustained activity was more difficult to establish if synapses were stronger (see above). This explains the missing data points in the corresponding regions of Figure 13. Stable network rates as low as 3.9 spikes per second, however, could be established for very large networks (350,000 neurons), bringing them close to the range of in vivo ongoing activity. It must be mentioned, however, that in this parameter regime, the increase in membrane conductance with respect to the resting state was considerably higher than found in vivo. Finally, note that all essential features of single-neuron and network behavior were retained in simulations of networks with three-fold and five-fold slower synapses.

4 Discussion

Networks with conductance-based synapses exhibit dynamic states similar to those demonstrated previously for networks with current-based synapses (Brunel, 2000; Mehring et al., 2003). However, there are also interesting and important differences. Most notably, the AI state with low firing rates reported by Brunel (2000) for current-based networks is often characterized by neuronal membrane potentials that are close to rest but tends to perform large and physiologically unrealistic excursions. By contrast, for networks with conductance-based synapses, the mean membrane potential remains only a few millivolts below threshold, and the size of the fluctuations is much smaller, consistent with in vivo intracellular recordings (Destexhe et al., 2003; Leger et al., 2005). We conclude that network models with conductance-based synapses provide a more realistic description of in vivo cortical activity at the level of membrane potentials.

It might appear as a straightforward corollary of our earlier results on single neurons with conductance-based synapses (Kuhn et al., 2004) that the mean membrane potential in network AI states should be close to the spike threshold. Spikes are induced by membrane potential fluctuations rather than by a drift of its mean, but the amplitude of these fluctuations is strongly attenuated due to the membrane impedance breakdown under massive synaptic bombardment. Therefore, if neurons in such networks produce spikes at all, it seems inevitable that the mean membrane potential should be close to the spike threshold. But why is it close to its resting value in current-based networks? The spectral properties of membrane potentials in the current-based model are characterized by a relatively large (fixed) membrane time constant, and irregular spiking can be obtained only with the help of a highly variable membrane potential. But to keep the firing rates low, the mean membrane potential must settle far away from threshold. However, matters are complicated by the fact that the mean membrane potential is a combined result of network dynamics and synaptic integration at the single-neuron level. For example, even small

correlations in the presynaptic population are known to dramatically alter the response properties of a neuron (Kuhn et al., 2003). We could show, however, that for low-rate AI states, input correlations and deviations from Poisson-like irregularity have only weak effects on individual membrane potentials, although some small but systematic shortcomings of the mean field predictions might find their explanation there. As a consequence, the simple self-consistency condition for firing rates employed by mean field theory suffices to correctly predict the mean firing rates and, consequently, the mean membrane potential of single neurons in recurrent networks.

Despite the large similarity of the respective state spaces for current-based and conductance-based networks, the precise combination of parameters that induce any particular dynamic state (external input ν_{ext}, and recurrent inhibition g) generally deviates between the current-based and the conductance-based model. One possible explanation for the observed distortions of the resulting parameter space lies in the slightly different definition of the parameter g for both models. For conductance-based networks, the effective PSP strength depends on both the level of membrane depolarization and, more importantly, the total intensity of the background activity (Kuhn et al., 2004). The static parameter g, in contrast, is defined as the relative amplitude of IPSPs with respect to EPSPs measured at rest. Therefore, the numerical values of g have a slightly different meaning in both models and cannot be directly compared. In principle, it would be possible to remap the parameter space defined by ν_{ext} and g such that the actual PSP strengths are taken into consideration. The obvious disadvantage of such a procedure is that the actual value of the alternative parameter, which would replace the control parameter g, can be determined only after the simulation because it depends, among other things, on the mean membrane potential.

In both current-based and conductance-based recurrent networks, inhibition plays a central role in shaping the dynamic state of the system. In both models, AI-type activity, which matches ongoing (spontaneous) activity in awake, behaving animals best (Softky & Koch, 1993; Abeles et al., 1990), is achieved only for relatively strong recurrent inhibition. Strong inhibition can be established by increasing the strength J_{inh} of inhibitory synapses (as we did) or, alternatively, increasing the excitability of inhibitory neurons (McCormick et al., 1985; Connors & Gutnick, 1990). The neurons in networks with weak inhibition fire at very high rates and produce very regular spike trains, and the network has a strong tendency to synchronize across the whole population. For approximate balance between recurrent excitation and inhibition, firing rates are low, the spike trains are quite irregular, and synchrony is broken. Only for very strong inhibition does the whole population tend to oscillate at low rates.

In our study, we mostly assumed identical synaptic time constants for excitatory and inhibitory synapses, in accordance with electrophysiological recordings in vitro (Fetz et al., 1991). Some researchers, however, report

inhibitory synapses that are slower than excitatory ones (Tarczy-Hornoch et al., 1998; Williams & Stuart, 2003). Interestingly, the only study addressing this issue in vivo failed to report any significant differences between excitation and inhibition and, in addition, the PSPs revealed there by spike-triggered averaging were generally much slower than in vitro (Matsumura et al., 1996). We can think of two different lines of argument that explain this apparent discrepancy. First, the unitary PSPs reported by Matsumura et al. (1996) are actually not unitary; rather, they reflect synchronous potentials induced by recurrent network dynamics. In this case they should not be directly compared to unitary PSPs measured in quiet networks in vitro. Second, there are no single synaptic couplings in the intact network in vivo; rather, one should assume multiple couplings with nonuniform delays. Such multiple synaptic couplings would effectively lead to compound PSPs that are much broader than those found in the reduced networks of cortical slices.

At present, the apparent inconsistencies between measurements in vivo and in vitro cannot be resolved. Therefore, we explored the effect of larger or asymmetric time constants on network dynamics by numerical simulation. We found that slower synapses (up to five-fold) do not change network dynamics in an essential way, provided excitatory and inhibitory synaptic time constants are approximately the same. If this is the case, a large part of the parameter space spanned by ν_{ext} and g is indeed occupied by low-rate AI states. By contrast, if inhibition is slower than excitation, firing rates are generally increased, as well as the regularity and synchrony in the network, even if the effective strength of all synapses at rest is unchanged. As a consequence, in the case of asymmetric time constants, the AI regime occupies a smaller fraction of the state space and eventually vanishes completely. It is possible, though, that increasing the heterogeneity of various parameters characterizing the network helps to partially restore AI-type activity in networks with slow inhibition (Denker, Timme, Diesmann, Wolf, & Geisel, 2004; Tetzlaff, Morrison, Timme, & Diesmann, 2005).

All the states of networks with random topology studied here exhibit some degree of synchrony. In extreme cases, synchronization appears in conjunction with global network oscillations; in other cases, the activity of individual neurons is irregular, and synchrony becomes visible only in cross-correlations averaged over many pairs. While the physical mechanism generating the correlations in each case is not clear in detail, several (mutually related) contributing factors can be listed. (1) common input induces correlations that may be quite strong. In fact, in a random network of 50,000 neurons, where each neuron has 5000 synapses, the overlapping population for any pair of neurons comprises 500 neurons on average, or 10% of each individual input population. (2) Uniform transmission delays were assumed for all synapses in the network ($D = 1.5$ ms). Such a system is bound to exhibit global oscillations of approximate period $4D$ (Murray, 2002; Brunel, 2000; Brunel & Wang, 2003; Maex & De Schutter, 2003; Roxin

et al., 2005). (3) Phase locking and synchronization are common phenomena in arrays of pulse coupled oscillators. Excitatory couplings induce a phase advance that, under very general assumptions, may lead to complete synchronization of all nodes in the system (Mirollo & Strogatz, 1990).

Many aspects of the collective states of a recurrent network with random synaptic topology are well described by a mean field model, based on averages across time and across the population of neurons. This has been demonstrated for the current-based model (Amit & Brunel, 1997), but as we showed here, it is also true for the conductance-based model. The mean field approach, though, may fail to predict with high accuracy the stationary firing rates in the network, depending on the degree of irregularity and synchrony expressed by the neurons in the network. Generally for AI network states, the mean field predictions were quite precise. However, networks exhibiting too regular or too synchronous activity did not match the predictions of the mean field model to the degree to which they deviated from our assumption that all inputs are independent Poisson processes (see Figures 4 and 9). Serious distortions of the rate transmission curves may be induced by such violations, and the shift of the fixed point may be of either sign, depending on the curvature of the transmission curve. Although a complete theory for such effects is currently not available, our scaling experiments for self-sustained activity (see Figure 12a) strongly indicate that the effects responsible for the deviations between network simulations and mean field theory do not depend on the size and architecture of the network.

From the mean field model of conductance-based neurons, one predicts a state of self-sustained asynchronous activity at low rates, even in the complete absence of external inputs. This result is essentially due to a peculiar property of single neurons with conductance-based synapses. The rate transfer function in the high-conductance state becomes nonmonotonic due to the shunting impedances of background activity (Kuhn et al., 2004). Numerical simulations of large spiking networks confirmed this prediction (see Figure 10), although the activity of smaller networks was found to be subject to spontaneous extinction as a result of activity fluctuations. The survival of the self-sustained state, however, improved with increasing network size (see Figure 11). The existence of a low-rate self-sustained state in the absence of external input is a distinguished property of conductance-based networks and is not shared by current-based networks. Likewise, in certain firing rate models (Wilson & Cowan, 1973), robust sustained activity at low rates is possible only if the network is either driven by external input or if it contains a certain fraction of endogenously active cells (Latham, Richmond, Nelson, et al., 2000; Latham, Richmond, Nirenberg, et al., 2000). Similar conclusions were drawn based on another model, where transient external stimuli induced a switching between two different network activity levels, but an external drive was still required for the network to exhibit sustained activity (Salinas, 2003). The firing rates attained during the self-sustained

activity states we described were very close to the rates predicted by the mean field model. Although independent of network size and simulation time step, the deviations in firing rate were systematic. Lower sustained activity of the recurrent network than predicted by the mean field theory was observed in conjunction with both high firing rates and strongly regular firing. Higher-than-predicted sustained activity, by contrast, was observed jointly with an increased amount of correlation (Bohte et al., 2000; Kuhn et al., 2003).

The lowest rate of self-sustained activity reached in this study was 3.9 spikes per second for a network of 350,000 neurons (see Figure 13a). To stabilize such low firing rates, the strength of inhibitory synapses had to be chosen exceedingly high ($g \approx 10$), leading to a mean membrane potential close to rest, and large fluctuations. The choice of relative strength of inhibitory synapses, though, seems justified in view of recent experimental studies (Williams & Stuart, 2002, 2003). Also, the effect of inhibition in pyramidal neurons is stronger, as most of the inhibitory synapses are located on the soma and the basal dendrites. In a point neuron model, this can be taken into account only by increasing the amplitude of inhibitory couplings. Moderate values for the synaptic amplitudes suffice if one arranges unequal time constants for excitatory and inhibitory conductances. In our networks, larger time constants for inhibition as reported for neocortical pyramidal neurons (Williams & Stuart, 2002, 2003) had a similar effect as increased amplitudes. Higher firing rates for inhibitory neurons (McCormick et al., 1985; Connors & Gutnick, 1990) would also lead to more effective inhibition.

Under which conditions real cortical networks share the properties of our model and whether the self-sustained network state is of biological relevance are unresolved issues. Nevertheless, experimental evidence pointing in this direction has been reported recently (Shu et al., 2003). A high level of ongoing activity without any specific stimulus has also been reported, for example, in the visual cortex (Arieli et al., 1996). Moreover, experiments of undercutting cortical tissue to deprive it from input first lead to a silent network, but activity could recur after a few days (Burns & Webb, 1979; Timofeev et al., 2000). Likewise, organotypic cultures of cortical neurons organize into an active network by developing strong enough recurrent synapses (Plenz & Aertsen, 1996).

Having shown that networks of spiking neurons can exhibit self-sustained activity at low firing rates in theory, the question arises which role this particular network state could play for the function of the mammalian neocortex. One possible scenario is that the self-sustained AI states provide the functional substrate into which other processes are embedded that eventually subserve higher brain functions. Processes based on spike synchronization (Abeles, 1991; Diesmann, Gewaltig, & Aertsen, 1999; Kumar, Rotter, & Aertsen, 2006) could be particularly effective in this context, since they have to merely "rearrange" the spikes generated by the

stable source of ongoing spontaneous activity. This would, among other things, shorten the response times and increase the sensitivity of the processing of inputs. Self-sustained activity in several distinct subnetworks, however, lends itself to the alternative interpretation of short-term memory, as proposed by Fuster (1973, 1988) Goldman-Rakic (1995), and others (Compte, Brunel, Goldman-Rakic, & Wang, 2000; Koulakov, Raghavachari, Kepecs, & Lisman, 2002; Brunel, 2003; McCormick et al., 2003). Also, the possibility of switching between different levels of activity by a very simple stimulus leads to the suggestion (Aertsen, Erb, & Palm, 1994; Salinas, 2003) that different contexts of neural processing could be represented by one and the same network in this way.

Acknowledgments

All numerical experiments have been carried out using the NEST simulation software (www.nest-initiative.org), and we thank Abigail Morrison for her advice on the simulation techniques. We also thank Markus Diesmann, Jens Kremkow, Birgit Kriener, Carsten Mehring, and Tom Tetzlaff for helpful discussions and Nicolas Brunel and Carl van Vreeswijk for their comments on an earlier version of the manuscript, as well as two anonymous referees for their insightful suggestions. We appreciate the technical support by the Freiburg Computing Center, in particular, Hans-Gunther Borrmann. This work was funded by GIF, DFG-GraKo, the 6th RFP of the EU (grant no. 15879-FACETS), and the BMBF (grant no. 01GQ0420 to the BCCN Freiburg).

References

Abeles, M. (1991). *Corticonics: neural circuits of the cerebral cortex.* Cambridge: Cambridge University Press.

Abeles, M., Vaadia, E., & Bergman, H. (1990). Firing patterns of single units in the prefrontal cortex and neural network models. *Network: Comput. Neural Systems, 1*, 13–25.

Abramowitz, M., & Stegun, I. A. (1964). *Handbook of mathematical functions*. Washington, DC: National Bureau of Standards.

Aertsen, A., Erb, M., & Palm, G. (1994). Dynamics of functional coupling in the cerebral cortex: An attempt at a model–based interpretation. *Physica D, 75*, 103–128.

Amit, D. J., & Brunel, N. (1997). Model of global spontaneous activity and local structured activity during delay periods in the cerebral cortex. *Cereb. Cortex, 7*, 237–252.

Arieli, A., Sterkin, A., Grinvald, A., & Aertsen, A. (1996). Dynamics of ongoing activity: Explanation of the large variability in evoked cortical responses. *Science, 273*(5283), 1868–1871.

Bernander, Ö., Douglas, R. J., Martin, K. A. C., & Koch, C. (1991). Synaptic background activity influences spatiotemporal integration in single pyramidal cells. *Proc. Natl. Acad. Sci. USA, 88*(24), 11569–11573.

Bohte, S. M., Spekreijse, H., & Roelfsema, P. R. (2000). The effects of pair-wise and higher-order correlations on the firing rate of a postsynaptic neuron. *Neural Comput., 12*, 153–179.

Braitenberg, V., & Schüz, A. (1998). *Cortex: Statistics and geometry of neuronal connectivity* (2nd ed.). Berlin: Springer-Verlag.

Brecht, M., & Sakmann, B. (2002). Dynamic representation of whisker deflection by synaptic potentials in spiny stellate and pyramidal cells in the barrels and septa of layer 4 rat somatosensory cortex. *J. Physiol. (Lond.), 543*, 49–70.

Brunel, N. (2000). Dynamics of sparsely connected networks of excitatory and inhibitory spiking neurons. *J. Comput. Neurosci., 8*(3), 183–208.

Brunel, N. (2003). Dynamics and plasticity of stimulus-selective persistent activity in cortical network models. *Cereb. Cortex, 13*(11), 1151–1161.

Brunel, N., & Wang, X.-J. (2003). What determines the frequency of fast network oscillations with irregular neural discharges? I. Synaptic dynamics and excitation-inhibition balance. *J. Neurophysiol., 90*, 415–430.

Burns, B. D., & Webb, A. C. (1979). The correlation between discharge times of neighbouring neurons in isolated cerebral cortex. *Proc. R. Soc. Lond. B., 203*(1115), 347–360.

Chance, F. S., Abbott, L. F., & Reyes, A. D. (2002). Gain modulation from background synaptic input. *Neuron, 35*, 773–782.

Chiu, C., & Weliky, M. (2001). Spontaneous activity in developing ferret visual cortex in vivo. *J. Neurosci., 21*, 8906–8914.

Compte, A., Brunel, N., Goldman-Rakic, P. S., & Wang, X. J. (2000). Synaptic mechanisms and network dynamics underlying spatial working memory in a cortical network model. *Cereb. Cortex, 10*(9), 910–923.

Connors, B. W., & Gutnick, M. J. (1990). Intrinsic firing patterns of diverse neocortical neurons. *TINS, 13*(3), 99–104.

Dayan, P., & Abbott, L. F. (2001). *Theoretical neuroscience*. Cambridge; MA: MIT Press.

Denker, M., Timme, M., Diesmann, M., Wolf, F., & Geisel, T. (2004). Breaking synchrony by heterogeneity in complex networks. *Phys. Rev. Lett., 92*(7), 074103.

Destexhe, A., Rudolph, M., & Paré, D. (2003). The high-conductance state of neocortical neurons in vivo. *Nat. Rev. Neurosci., 4*, 739–751.

Diesmann, M., & Gewaltig, M.-O. (2002). NEST: An environment for neural systems simulations. In T. Plesser & V. Macho (Eds.), *Forschung und wisschenschaftliches Rechnen, Beiträge zum Heinz-Billing-Preis 2001* (pp. 43–70). Göttingen: Ges. für Wiss. Datenverarbeitung.

Diesmann, M., Gewaltig, M.-O., & Aertsen, A. (1999). Stable propagation of synchronous spiking in cortical neural networks. *Nature, 402*(6761), 529–533.

Fetz, E., Toyama, K., & Smith, W. (1991). Synaptic interactions between cortical neurons. In A. Peters (Ed.), *Cerebral cortex* (pp. 1–47). New York: Plenum Press.

Fuster, J. M. (1973). Unit activity in prefrontal cortex during delayed-response performance: Neuronal correlates of transient memory. *J. Neurophysiol., 36*(1), 61–78.

Fuster, J. M. (1988). *The prefrontal cortex*. New York: Raven Press.

Galassi, M., Davies, J., Theiler, J., Gough, B., Jungman, G., Booth, M., & Rossi, F. (2001). *GNU scientific library: Reference manual*. Bristol: Network Theory Limited.

Gerstein, G. L., & Mandelbrot, B. (1964). Random walk models for the spike activity of a single neuron. *Biophys. J., 4*, 41–68.

Gerstner, W., & Kistler, W. (2002). *Spiking neuron models: Single neurons, populations, plasticity*. Cambridge: Cambridge University Press.

Goldman-Rakic, P. S. (1995). Cellular basis of working memory. *Neuron, 14*, 477–485.

Golomb, D., & Hansel, D. (2000). The number of synaptic inputs and the synchrony of large, sparse neuronal networks. *Neural Comput., 12*, 1095–1139.

Hansel, D., Mato, G., Meunier, C., & Neltner, L. (1998). On numerical simulations of integrate-and-fire neural networks. *Neural Comput., 10*(2), 467–483.

Hasenstaub, A., Shu, Y., Haider, B., Kraushaar, U., Duque, A., & McCormick, D. (2005). Inhibitory postsynaptic potentials carry synchronized frequency information in active cortical networks. *Neuron, 3*(47), 423–435.

Jack, J. J. B., Noble, D., & Tsien, R. W. (1975). *Electric current flow in excitable cells*. Oxford: Clarendon Press.

Knuth, D. E. (1997). *The art of computer programming: Seminumerical algorithms* (3rd ed.). Reading, MA: Addison-Wesley.

Koulakov, A. A., Raghavachari, S., Kepecs, A., & Lisman, J. E. (2002). Model for a robust neural integrator. *Nat. Neurosci., 5*(8), 775–782.

Kuhn, A., Aertsen, A., & Rotter, S. (2003). Higher-order statistics of input ensembles and the response of simple model neurons. *Neural Comput., 15*(1), 67–101.

Kuhn, A., Aertsen, A., & Rotter, S. (2004). Neuronal integration of synaptic input in the fluctuation-driven regime. *J. Neurosci., 24*(10), 2345–2356.

Kumar, A., Rotter, S., & Aertsen, A. (2006). Propagation of synfire activity in locally connected networks with conductance-based synapses. In *Computational and Systems Neuroscience (Cosyne) 2006*. Available online at http://cosyne.org/wiki/cosyne_06.

Kumar, A., Schrader, S., Rotter, S., & Aertsen, A. (2005). Dynamics of random networks of spiking neurons with conductance-based synapses. In *Computational and Systems Neuroscience (Cosyne) 2005* (p. 153). Available online at http://cosyne.org/wiki/Cosyne_05.

Latham, P. E., Richmond, B. J., Nelson, P. G., & Nirenberg, S. (2000). Intrinsic dynamics in neuronal networks. I. Theory. *J. Neurophysiol., 83*, 808–827.

Latham, P. E., Richmond, B. J., Nirenberg, S., & Nelson, P. G. (2000). Intrinsic dynamics in neuronal networks. II. Experiment. *J. Neurophysiol., 83*, 828–835.

Leger, J., Stern, E., Aertsen, A., & Heck, D. (2005). Synaptic integration in rat frontal cortex shaped by network activity. *J. Neurophysiol., 1*(93), 281–293.

Maex, R., & De Schutter, E. (2003). Resonant synchronization in heterogeneous networks of inhibitory neurons. *J. Neurosci., 23*(33), 10503–10514.

Markram, H., Toledo-Rodriguez, M., Wang, Y., Gupta, A., Silberberg, G., & Wu, C. (2004). Interneurons of the neocortical inhibitory system. *Nat. Rev. Neurosci., 5*(10), 793–807.

Matsumura, M., Chen, D., Sawaguchi, T., Kubota, K., & Fetz, E. E. (1996). Synaptic interactions between primate precentral cortex neurons revealed by spike-triggered averaging of intracellular membrane potentials in vivo. *J. Neurosci., 16*(23), 7757–7767.

McCormick, D. A., Connors, B. W., Lighthall, J. W., & Prince, D. A. (1985). Comparative electrophysiology of pyramidal and sparsely spiny neurons of the neocortex. *J. Neurophysiol., 54*(4), 782–806.

McCormick, D. A., Shu, Y., Hasenstaub, A., Sanchez-Vives, M., Badoual, M., & Bal, T. (2003). Persistent cortical activity: Mechanisms of generation and effects on neuronal excitability. *Cereb. Cortex, 13*(11), 1219–1231.

Meffin, H., Burkitt, A. N., & Grayden, D. B. (2004). An analytical model for the large, fluctuating synaptic conductance state typical of neocortical neurons *in vivo*. *J. Comput. Neurosci., 16*, 159–175.

Mehring, C., Hehl, U., Kubo, M., Diesmann, M., & Aertsen, A. (2003). Activity dynamics and propagation of synchronous spiking in locally connected random networks. *Biol. Cybern., 88*(5), 395–408.

Mirollo, R. E., & Strogatz, S. H. (1990). Synchronization of pulse-coupled biological oscillators. *SIAM J. Appl. Math., 50*(6), 1645–1662.

Morrison, A., Hake, J., Straube, S., Plesser, H. E., & Diesmann, M. (2005). Precise spike timing with exact subthreshold integration in discrete time network simulations. In *Proceedings of the 30th Göttingen Neurobiology Conference* (p. 205B). Available online at http://cosyne.org/wiki/cosyne_05.

Morrison, A., Mehring, C., Geisel, T., Aertsen, A., & Diesmann, M. (2005). Advancing the boundaries of high connectivity network simulation with distributed computing. *Neural Comput., 17*(8), 1776–1801.

Murray, J. D. (2002). *Mathematical biology. I: An introduction* (3rd ed.). Berlin: Springer.

Nawrot, M. P., Riehle, A., Aertsen, A., & Rotter, S. (2000). Spike count variability in motor cortical neurons. *European Journal of Neuroscience*, *12*, 506.

Plenz, D., & Aertsen, A. (1996). Neural dynamics in cortex-striatum co-cultures II—spatiotemporal characteristics of neuronal activity. *Neuroscience, 70*(4), 893–924.

Press, W. H., Teukolsky, S. A., Vetterling, W. T., & Flannery, B. P. (1992). *Numerical recipes in C* (2nd ed.). Cambridge: Cambridge University Press.

Rapp, M., Yarom, Y., & Segev, I. (1992). The impact of parallel fiber background activity on the cable properties of cerebellar Purkinje cells. *Neural Comput., 4*, 518–533.

Rauch, A., La Camera, G., Lüscher, H., Senn, W., & Fusi, S. (2003). Neocortical pyramidal cells respond as integrate-and-fire neurons to in vivo like input currents. *J. Neurophysiol., 90*, 1598–1612.

Rotter, S., & Diesmann, M. (1999). Exact digital simulation of time-invariant linear systems with applications to neuronal modeling. *Biol. Cybern., 81*(5/6), 381–402.

Roxin, A., Brunel, N., & Hansel, D. (2005). The role of delays in shaping spatiotemporal dynamics of neuronal activity in large networks. *Phys. Rev. Lett., 94*(23), 238103.

Salinas, E. (2003). Background synaptic activity as a switch between dynamic states in network. *Neural Comput., 15*, 1439–1475.

Schrader, S., Kumar, A., Rotter, S., & Aertsen, A. (2005). Dynamics of self-sustained activity. In *Proceedings of the 30th Göttingen Neurobiology Conference*. Available at http://www.neuro.uni-goettingen.de/nbc.php?sel=archiv.

Shadlen, M. N., & Newsome, W. T. (1998). The variable discharge of cortical neurons: Implications for connectivity, computation, and information coding. *J. Neurosci., 18*(10), 3870–3896.

Shelley, M., McLaughlin, D., Shapley, R., & Wielaard, J. (2002). States of high conductance in a large-scale model of the visual cortex. *J. Comput. Neurosci., 13*(2), 93–109.

Shu, Y., Hasenstaub, A., & McCormick, D. A. (2003). Turning on and off recurrent balanced cortical activity. *Nature, 423*(6937), 288–293.

Softky, W. R., & Koch, C. (1993). The highly irregular firing of cortical cells is inconsistent with temporal integration of random EPSPs. *J. Neurosci., 13*(1), 334–350.

Stroeve, S., & Gielen, S. (2001). Correlation between uncoupled conductance-based integrate-and-fire neurons due to common and synchronous presynaptic firing. *Neural Comput., 13*(9), 2005–2029.

Tarczy-Hornoch, K., Martin, K. A. C., Jack, J. J. B., & Stratford, K. J. (1998). Synaptic interactions bewteen smooth and spiny neurones in layer 4 of cat visual cortex in vitro. *J. Physiol. (Lond.), 508*(2), 351–363.

Tetzlaff, T., Morrison, A., Timme, M., & Diesmann, M. (2005). Heterogeneity breaks global synchrony in large networks. In *Proceedings of the 30th Göttingen Neurobiology Conference*. Available online at http://www.neuro.unigoettingen.de/nbc.php?sel=archiv.

Tetzlaff, T., Rotter, S., Stark, E., Abeles, M., Aertsen, A., & Diesmann, M. (2007). *Time scale dependence of neuronal connections*. Manuscript submitted for publication.

Timofeev, I., Grenier, F., Bazhenov, M., Sejnowski, T. J., & Steriade, M. (2000). Origin of slow cortical oscillations in deafferented cortical slabs. *Cereb. Cortex, 10*(12), 1185–1199.

Tuckwell, H. C. (1988a). *Introduction to theoretical neurobiology* (Vol. 1). Cambridge: Cambridge University Press.

Tuckwell, H. C. (1988b). *Introduction to theoretical neurobiology* (Vol. 2). Cambridge: Cambridge University Press.

Vaadia, E., & Aertsen, A. (1992). Coding and computation in the cortex: Single-neuron activity and cooperative phenomena. In A. Aertsen & V. Braitenberg (Eds.), *Information processing in the cortex: Experiments and theory* (pp. 81–121). Berlin: Springer-Verlag.

van Vreeswijk, C., & Sompolinsky, H. (1998). Chaotic balanced state in a model of cortical circuits. *Neural Comput., 10*, 1321–1371.

Vogels, T. P., & Abbott, L. F. (2005). Signal propagation and logic gating in networks of integrate-and-fire neurons. *J. Neurosci., 25*(46), 10786–10795.

Vogels, T. P., Rajan, K., & Abbott, L. F. (2005). Neural network dynamics. *Annu. Rev. Neurosci., 28*, 357–376.

Williams, S. R., & Stuart, G. J. (2002). Dependence of EPSP efficacy on synaptic location in neocortical pyramidal neurons. *Science, 295*, 1907–1910.

Williams, S. R., & Stuart, G. J. (2003). Voltage- and site-dependent control of the somatic impact of dendritic IPSPs. *J. Neurosci., 23*(19), 7358–7367.

Wilson, H. R., & Cowan, J. D. (1973). A mathematical theory of the functional dynamics of cortical and thalamic nervous tissue. *Kybernetik, 13*, 55–80.

Received June 28, 2006; accepted February 13, 2007.